Mathematics

https://www.aimspress.com/journal/Math

AIMS Mathematics, 11(7): 19593–19632.
DOI: 10.3934/math.2026796
Received: 26 March 2026
Revised: 13 June 2026
Accepted: 18 June 2026
Published: 03 July 2026

Research article

A new logarithmic Lomax–Rayleigh distribution: properties, simulation, and applications

Huda Mohammed Alomari*

Department of Mathematics, Faculty of Science, Al-Baha University, Al-Baha, Saudi Arabia

* **Correspondence:** Email: haldrawshah@bu.edu.sa; Tel: +966531972717.

Abstract: This paper introduces the logarithmic Lomax–Rayleigh (Log-LR) distribution, a new three-parameter lifetime model within the Lomax–G family, proposed to provide enhanced flexibility for modeling skewed and heavy-tailed data arising in reliability and survival analysis. The model adopts the Rayleigh distribution as the baseline and incorporates two additional shape parameters. The resulting hazard rate function (HRF) is highly flexible and can exhibit inverse-J and non-monotonic decreasing–increasing shapes depending on the parameter values, making the model suitable for a wide range of lifetime data. Several fundamental statistical properties are derived, including the probability density function, cumulative distribution function (CDF), reliability and hazard functions, cumulative and reverse hazard rates, the quantile function, Shannon entropy, and the mean residual life function (MRL). The r-th moments and L-moments are expressed in integral form and evaluated numerically. Additional characteristics, including the moment generating function (MGF), skewness, kurtosis, and order statistics, are also investigated. The model parameters are estimated via maximum likelihood, and a Monte Carlo simulation study is conducted to assess the consistency and efficiency of the estimators across different sample sizes. The practical usefulness of the Log-LR distribution is illustrated using four real datasets. Goodness-of-fit comparisons, based on log-likelihood, Akaike Information Criterion (AIC), Bayesian Information Criterion (BIC), and Kolmogorov–Smirnov (KS), Anderson-Darling (AD), and Cramér-von Mises (CvM) statistics together with their corresponding p-values, are performed against nine competing models. The results consistently demonstrate that the proposed Log-LR distribution outperforms the competing models, highlighting its effectiveness as a flexible alternative for modeling lifetime data.

Keywords: logarithmic Lomax–Rayleigh distribution; hazard function; probability density function; cumulative distribution function; maximum likelihood estimation; simulation study; statistical modeling; lifetime data
Mathematics Subject Classification: 62E10, 62F10, 62N05

1. Introduction

In many practical applications, classical distributions, such as the Exponential, Gamma, and Beta models serve as standard tools for analyzing lifetime data. However, these models often lack the flexibility required to capture complex features commonly encountered in real-world data, including heavy tails and early-life failures. This limitation has motivated the development of extended distributional families through transformation, compounding, and parameter-induction techniques that offer greater control over skewness, kurtosis, and tail behavior.

A fundamental contribution in this direction was made by [1], who proposed the Beta-normal distribution via a logit transformation of a Beta-distributed variable. Building on this idea, [2] introduced a general method for adding parameters to existing distributions. Since then, numerous G-family generators have been developed, including the Burr XII-G family [3], the Weibull-G family [4], the Gompertz-G family [5], and the odd Chen-G family [6], among others (see also [7–9]).

Within the Lomax-based family, several notable extensions have been proposed. [10] introduced the Gamma–Lomax distribution as a flexible three-parameter model. [11] generalized the power distribution using the quadratic rank transmutation map, while [12] developed a Lomax-G framework based on a Beta-generated transformation. More recently, [13] proposed the Lomax–tangent Weibull distribution and studied its mathematical properties, and [14] introduced a bivariate Lomax-G family within the Farlie-Gumbel-Morgenstern (FGM) copula framework. Additionally, [15] proposed a bivariate power Lomax distribution within the Sarmanov framework and studied its reliability properties. In a related line of research, recent advances in degradation-based reliability modeling have attracted considerable attention; see, for example, [16–18] for Bayesian-and Wiener-process-based methodologies.

Despite these advances, most existing Lomax-based models are not specifically designed to capture bathtub-shaped hazard rates that arise in systems subject to both early-life failures and late-life wear-out. In addition, many of these extensions require four or more parameters, increasing the risk of overfitting and limiting the interpretability. There is therefore a need for a simpler yet flexible model that can describe such failure-rate patterns with fewer parameters.

The logarithmic Lomax–Rayleigh (Log-LR) distribution is more flexible than other extensions of the Lomax and Rayleigh distributions because it applies a logarithmic Lomax-type transformation to the Rayleigh baseline rather than simply adding shape parameters. This method gives a simple, flexible, and mathematically tractable model. Closed-form expressions for the cumulative distribution, probability density, hazard rate, reverse hazard rate, and quantile functions facilitate theoretical analysis, parameter estimation, and random value generation. The Rayleigh distribution is obtained as a special case of the Log-LR model under specific parameter settings. The Log-LR distribution models various hazard-rate patterns, including decreasing and bathtub-shaped curves common in reliability and survival analyses. These characteristics make it a versatile and effective tool for lifetime data analysis. A comparison of selected Lomax- and Rayleigh-based lifetime distributions is presented in Table 1.

Table 1. Comparison of selected Lomax- and Rayleigh-based lifetime distributions.

Distribution	Params	Dec HRF	BT HRF	Closed-form Quantile	Rayleigh Limit
Gamma–Lomax [10]	3	×	✓	✓	×
Gumbel–Lomax [19]	4	✓	✓	✓	×
Alpha Power Lomax [20]	3	✓	×	✓	×
New Weibull–Rayleigh [21]	4	✓	✓	✓	✓
Gen. Inv. Kum.–Rayleigh [22]	4	✓	✓	✓	✓
Log-LR (proposed)	3	✓	✓	✓	✓

Note: Dec = monotonically decreasing, BT = bathtub-shaped.

The Rayleigh distribution is a natural choice as a baseline for this purpose. It has a single parameter, a closed-form cumulative distribution function (CDF), and a well-understood structure. By embedding it within a logarithmic Lomax generator, we obtain a three-parameter family that retains analytical simplicity while gaining the ability to model inverse-J and non-monotonic decreasing–increasing hazard rate patterns.

Accordingly, the main contributions of this paper are as follows.

(1) A new three-parameter lifetime model, termed the Log-LR distribution, is introduced. The model possesses a flexible hazard rate function (HRF) that can exhibit inverse-J and non-monotonic decreasing–increasing shapes, making it suitable for modeling a wide range of lifetime data.

(2) Key statistical properties are derived in closed form, including probability density function (PDF), CDF, reliability and HRFs, and order statistics. The raw moments are expressed as integral representations and evaluated numerically, along with the moment-generating function (MGF), skewness, and kurtosis.

(3) A Monte Carlo simulation study demonstrates the consistency and the efficiency of maximum likelihood estimators (MLEs) across a range of parameter settings and sample sizes.

(4) The practical superiority of the proposed Log-LR model is demonstrated through its application to four real datasets. It outperforms nine competing lifetime distributions, namely the Rayleigh, Weibull, Gamma, Lomax, logistic Lomax, logistic inverse Lomax, generalized inverse Rayleigh, Gumbel–Lomax (GL), and Alpha power Lomax (APL) distributions. Model comparison is based on information criteria (Akaike Information Criterion (AIC) and Bayesian Information Criterion (BIC)), maximized log-likelihood, and goodness-of-fit tests including the Kolmogorov–Smirnov (KS), Anderson–Darling (AD), and Cramér–von Mises (CvM) statistics, along with their corresponding p-values.

The remainder of this paper is organized as follows. Section 2 presents the Log-LR distribution and its mathematical properties. Section 3 derives the order statistics. Sections 4 and 5 address parameter estimation and simulation, respectively. Section 6 illustrates the model using four real datasets, and Section 7 concludes the paper.

2. The logarithmic Lomax–Rayleigh (Log-LR) distribution

In this section, we introduce the three-parameter Log-LR distribution and derive its key statistical properties.

2.1. Definition

A random variable X is said to follow the Logarithmic Lomax–G family if its CDF is given by

$$G(x) = \left(\frac{\beta}{\beta - \log F(x)}\right)^{\alpha}, \tag{2.1}$$

where $F(x)$ is the baseline CDF, $\alpha > 0$ and $\beta > 0$ are shape parameters, and $\beta - \log F(x) > 0$ for all $x > 0$. The corresponding PDF is obtained by differentiating (2.1) with respect to x:

$$g(x) = \frac{\alpha \beta^{\alpha} f(x)}{F(x)} \left[\beta - \log F(x)\right]^{-(\alpha+1)}, \tag{2.2}$$

where $f(x) = dF(x)/dx$ is the baseline PDF. For further details on the Lomax-G family, see [12].

In this study, the Rayleigh distribution is adopted as the baseline. A continuous random variable X follows the Rayleigh distribution with scale parameter $\lambda > 0$ if its CDF and PDF are, respectively,

$$F(x; \lambda) = 1 - e^{-x^2/(2\lambda^2)}, \qquad x \geq 0, \tag{2.3}$$

$$f(x; \lambda) = \frac{x}{\lambda^2} e^{-x^2/(2\lambda^2)}. \tag{2.4}$$

Substituting Eq (2.3) into Eq (2.1), the CDF of the Log-LR distribution with parameter vector $\boldsymbol{\omega} = (\alpha, \beta, \lambda)$ is

$$G(x; \boldsymbol{\omega}) = \left(\frac{\beta}{\eta(x)}\right)^{\alpha}, \qquad x > 0. \tag{2.5}$$

Similarly, substituting Eqs (2.3) and (2.4) into Eq (2.2), the PDF of the Log-LR distribution is

$$g(x; \boldsymbol{\omega}) = \frac{\alpha \beta^{\alpha} x \, e^{-x^2/(2\lambda^2)}}{\lambda^2 (1 - e^{-x^2/(2\lambda^2)})} \left[\eta(x)\right]^{-(\alpha+1)}, \tag{2.6}$$

where $\alpha > 0, \beta > 0, \lambda > 0$, and $\eta(x) = \beta - \log(1 - e^{-x^2/(2\lambda^2)})$.

Parameter interpretation

- **Shape parameter** (α)**:** The parameter (α) influences the distribution's shape through the term $\eta(x)^{-(\alpha+1)}$. Higher values of (α) increase the concentration of probability mass near the mode, and the right tail becomes lighter. (α) also plays a key role in defining the HRF, which may decrease or exhibit a bathtub shape.
- **Shape parameter** (β)**:** The parameter (β) influences the distribution through

  $$\eta(x) = \beta - \log\left(1 - e^{-x^2/(2\lambda^2)}\right).$$

  β plays an important role in determining how probability mass is distributed. Smaller values of β result in greater concentration near the lower tail, whereas larger values produce a wider spread of observations and a smoother hazard rate.

- **Scale parameter** (λ)**:** Inherited from the Rayleigh baseline distribution, (λ) controls the overall scale of the distribution. Specifically, if

$$X \sim \text{Log-LR}(\alpha, \beta, \lambda),$$

then

$$cX \sim \text{Log-LR}(\alpha, \beta, c\lambda), \qquad c > 0,$$

showing that (λ) is a scale parameter.

Figure 1 illustrates these effects for selected parameter combinations.

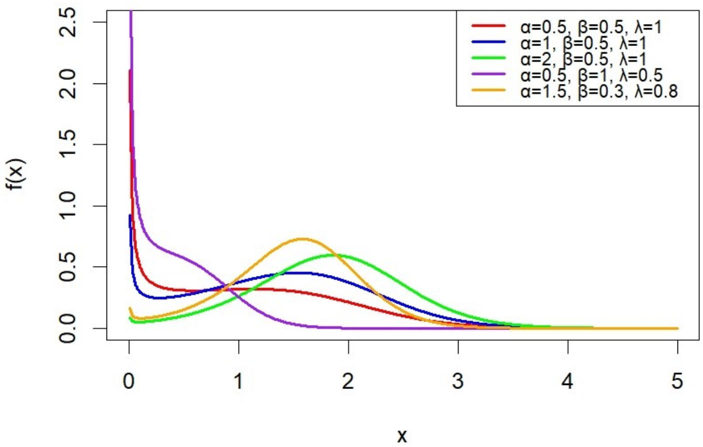

Figure 1. PDF of the Log-LR distribution for selected parameter values.

Remark. *As $\alpha = \beta \to \infty$, the Log-LR distribution reduces to the Rayleigh distribution with the same scale parameter λ. More generally, the same limit holds whenever $\alpha, \beta \to \infty$ with $\alpha/\beta \to 1$.*

Proof. Let $z = -\log F_R(x) > 0$, where $F_R(x; \lambda) = 1 - e^{-x^2/(2\lambda^2)}$ is the Rayleigh CDF. The Log-LR CDF can be written as

$$G(x) = \left(\frac{\beta}{\beta + z}\right)^{\alpha} = \left(1 + \frac{z}{\beta}\right)^{-\alpha}.$$

Setting $\alpha = \beta$ and letting $\alpha \to \infty$,

$$G(x) = \left(1 + \frac{z}{\alpha}\right)^{-\alpha} \xrightarrow{\alpha \to \infty} e^{-z} = e^{\log F_R(x)} = F_R(x; \lambda),$$

which is exactly the Rayleigh CDF with scale parameter λ. More generally, writing $G(x) = \exp(-\alpha \log(1 + z/\beta)) \approx \exp(-\alpha z/\beta)$, the limit equals $e^{-z} = F_R(x; \lambda)$ when $\alpha/\beta \to 1$. □

2.2. *Related functions*

Reliability (survival) function.

$$R(x; \omega) = 1 - G(x; \omega) = 1 - \left(\frac{\beta}{\eta(x)}\right)^{\alpha}. \tag{2.7}$$

Hazard rate function (HRF). The HRF, defined as $h(x) = g(x)/[1 - G(x)]$, takes the form

$$h(x;\omega) = \frac{\alpha\,\beta^{\alpha}\,x\,e^{-x^2/(2\lambda^2)}}{\lambda^2(1 - e^{-x^2/(2\lambda^2)})\,\eta(x)}\,[\eta(x)^{\alpha} - \beta^{\alpha}]. \tag{2.8}$$

As shown in Figure 1, the PDF of the Log-LR distribution exhibits various shapes depending on the parameter values. The parameters α and β primarily determine the shape of the density and hazard functions by controlling the peakedness and the behavior of the tail, while the scale parameter λ controls the distribution dispersion. Figure 2 shows HRF under different parameter configurations. The results indicate that the proposed distribution accommodates diverse hazard behaviors, including inverse-J and non-monotonic decreasing–increasing shapes, demonstrating its suitability for modeling complex lifetime and reliability data.

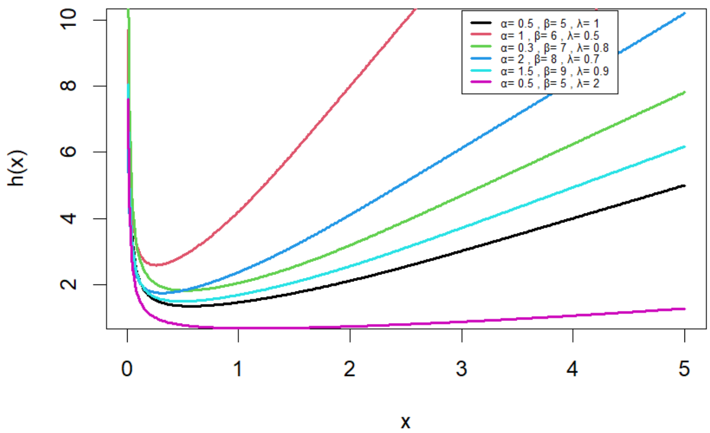

Figure 2. HRF of the Log-LR distribution for selected parameter values.

Cumulative hazard function.

$$H(x;\omega) = -\log R(x;\omega) = -\log\left[1 - \left(\frac{\beta}{\eta(x)}\right)^{\alpha}\right].$$

Reverse hazard rate function. The reverse HRF, defined as $\tau(x) = g(x)/G(x)$, is given by

$$\tau(x;\omega) = \frac{\alpha\,x\,e^{-x^2/(2\lambda^2)}}{\lambda^2(1 - e^{-x^2/(2\lambda^2)})\,\eta(x)}.$$

2.3. Hazard rate shape analysis

The HRF of the Log-LR distribution, given in Eq (2.8), can take different shapes depending on the parameter values. From the asymptotic analysis, $h(x) \to \infty$ as $x \to 0^+$ and $h(x) \sim x/\lambda^2$ as $(x \to \infty)$ for all admissible parameter values. Therefore, the hazard rate diverges to infinity at both boundaries of its support. Since $h(x)$ is continuous on $(0, \infty)$ and tends to infinity as $x \to 0^+$ and $x \to \infty$, it must attain at least one global minimum at some point $x_{\min} > 0$. Although all hazard functions in this family have this minimum, the practical distinction between different shapes depends on the extent to which the hazard rate increases after reaching it. To quantify this behavior, we introduce

$$\mathcal{R} = \frac{h(x_{\text{right}})}{h(x_{\min})}.$$

Here, x_{right} is a large value in the right tail of the distribution. Values of $\mathcal{R}$ close to unity indicate that the hazard rate remains near its minimum in the right tail, whereas larger values of $\mathcal{R}$ correspond to a more substantial increase beyond the minimum, yielding a more pronounced bathtub-shaped pattern. The index $\mathcal{R}$ is a useful way to differentiate nearly monotone hazard functions from those that are clearly bathtub-shaped. Figure 3 shows the classification regions.

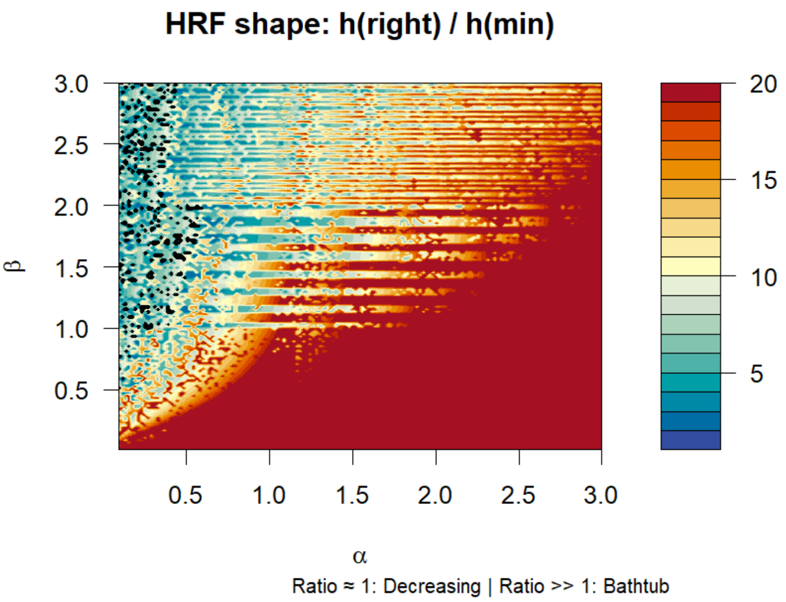

Figure 3. Contour plot of the hazard-rate shape ratio $\mathcal{R} = h(x_{\text{right}})/h(x_{\min})$ in the (α, β)-plane for $\lambda = 1$. Blue and green regions ($\mathcal{R} \approx 1$) correspond to an approximately decreasing hazard rate, whereas orange and red regions ($\mathcal{R} \gg 1$) indicate a pronounced bathtub-shaped hazard rate.

2.4. *Quantile function*

The quantile function is obtained by inverting the CDF Eq (2.5):

$$Q(u) = \lambda \sqrt{-2 \log[1 - \exp(\beta - \beta\, u^{-1/\alpha})]}, \qquad 0 < u < 1. \tag{2.9}$$

The median is obtained by setting $u = 0.5$:

$$\text{Median} = Q(0.5) = \lambda \sqrt{-2 \log[1 - \exp(\beta - \beta\, (0.5)^{-1/\alpha})]}.$$

The Bowley skewness and Moors kurtosis coefficients based on quantiles are shown in Figure 4 and are defined, respectively, as follows:

$$\text{Skewness (Bowley)} = \frac{Q(3/4) + Q(1/4) - 2\,Q(1/2)}{Q(3/4) - Q(1/4)},$$

$$\text{Kurtosis (Moors)} = \frac{Q(7/8) - Q(5/8) + Q(3/8) - Q(1/8)}{Q(3/4) - Q(1/4)}.$$

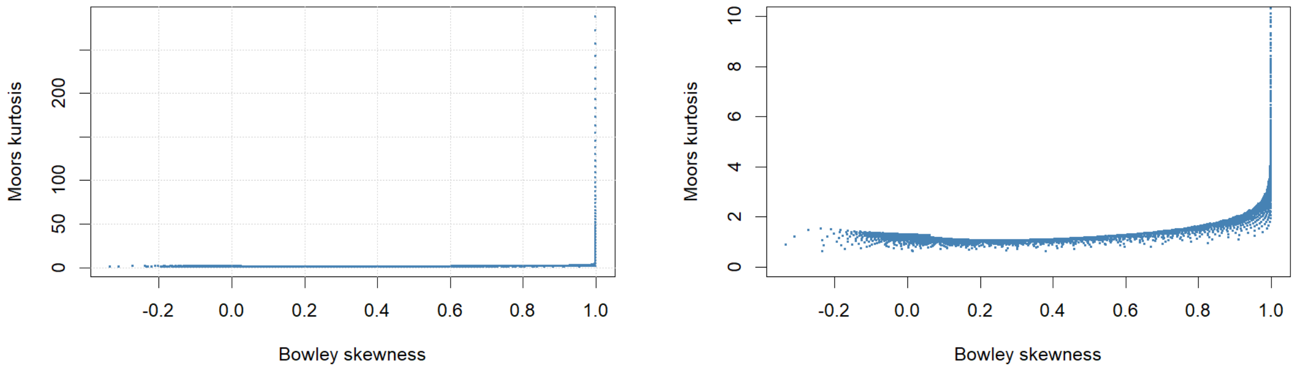

Figure 4. Variation diagram of Bowley skewness versus Moors kurtosis for the Log-LR distribution across $\alpha \in (0.2, 5)$ and $\beta \in (0.01, 5)$ with $\lambda = 1$. Left: full range. Right: zoomed view (Moors kurtosis ≤ 10).

2.5. *Moments*

The r-th raw moment of the Log-LR distribution is given by

$$E(X^r) = \alpha\beta^\alpha \int_0^\infty \frac{x^{r+1} e^{-x^2/(2\lambda^2)}}{\lambda^2 \left(1 - e^{-x^2/(2\lambda^2)}\right)} [\eta(x)]^{-(\alpha+1)} dx. \tag{2.10}$$

Using the transformation

$$y = -\log\left(1 - e^{-x^2/(2\lambda^2)}\right),$$

this implies

$$1 - e^{-x^2/(2\lambda^2)} = e^{-y}, \qquad e^{-x^2/(2\lambda^2)} = 1 - e^{-y}.$$

Then the r-th raw moment in Eq (2.10) can be written as

$$E(X^r) = \alpha\beta^\alpha (2\lambda^2)^{r/2} \int_0^\infty [-\log(1 - e^{-y})]^{r/2} (\beta + y)^{-(\alpha+1)}\, dy. \tag{2.11}$$

Using the known expansion

$$-\log(1 - e^{-y}) = \sum_{k=1}^{\infty} \frac{e^{-ky}}{k}, \qquad y > 0,$$

we obtain

$$[-\log(1 - e^{-y})]^{r/2} = \left(\sum_{k=1}^{\infty} \frac{e^{-ky}}{k}\right)^{r/2}.$$

For general values of r, the resulting expression does not appear to simplify to a finite combination of elementary functions or standard special functions. Consequently, no tractable closed-form expression for the raw moments was found, so numerical integration is employed to evaluate them. Truncated series expansions may also be used to obtain accurate approximations. For more details, see Appendix A.

Variance

The variance is given by

$$\mathrm{Var}(X) = E(X^2) - [E(X)]^2,$$

where the moments are computed using Eq (2.11).

2.6. Moment generating function

The MGF of a random variable X is defined as

$$M_X(t) = E\left(e^{tX}\right) = \int_0^{\infty} e^{tx} g(x)\,dx, \qquad t \in \mathcal{D},$$

where $g(x)$ denotes the density function of the Log-LR distribution and $\mathcal{D}$ is the set of values of t for which the integral exists. Equivalently, when the moments exist in a neighborhood of zero, the MGF can be expressed as the following formal power series:

$$M_X(t) = \sum_{r=0}^{\infty} \frac{t^r}{r!} E(X^r), \qquad t \text{ in a neighborhood of } 0. \tag{2.12}$$

To investigate the existence of the MGF, we study the tail behavior of the Log-LR density. As $x \to \infty$, we have

$$1 - \exp\left(-\frac{x^2}{2\lambda^2}\right) \to 1, \qquad \eta(x) \to \beta,$$

and therefore the density satisfies

$$g(x) \sim \frac{\alpha}{\beta\lambda^2}\, x \exp\left(-\frac{x^2}{2\lambda^2}\right), \qquad x \to \infty.$$

Hence, for large x,

$$e^{tx} g(x) = O\left(x \exp\left(tx - \frac{x^2}{2\lambda^2}\right)\right).$$

Completing the square yields

$$tx - \frac{x^2}{2\lambda^2} = -\frac{(x - \lambda^2 t)^2}{2\lambda^2} + \frac{\lambda^2 t^2}{2},$$

which implies that

$$e^{tx} g(x) \le C\, x \exp\left(-\frac{(x - \lambda^2 t)^2}{2\lambda^2}\right)$$

for some constant $C > 0$. Since the right-hand side is integrable over $(0, \infty)$ for all $t \in \mathbb{R}$, it follows that

$$\int_0^{\infty} e^{tx} g(x)\,dx < \infty, \qquad \forall\, t \in \mathbb{R}.$$

Consequently, the MGF exists for all real values of t under the regularity conditions on the density, and all positive integer moments of the distribution are finite. Finally, substituting Eq (2.11) into Eq (2.12) yields the series representation

$$M_X(t) = \sum_{r=0}^{\infty} \frac{t^r}{r!}\, \alpha\beta^{\alpha} (2\lambda^2)^{r/2} \int_0^{\infty} [-\log(1 - e^{-y})]^{r/2} (\beta + y)^{-(\alpha+1)}\, dy.$$

No closed-form expression appears to be available for this representation, and its numerical evaluation requires either truncating the series or performing direct numerical integration.

2.7. L-moments

L-moments are useful summary measures of a distribution and provide robust descriptions of location, dispersion, skewness, and tail behavior. For a random variable with quantile function $Q(u)$, the r-th L-moment is defined by [23]

$$\ell_r = \frac{1}{r}\sum_{k=0}^{r-1}(-1)^k\binom{r-1}{k}\int_0^1 u^{r-1-k}(1-u)^k Q(u)\,du. \tag{2.13}$$

The first four L-moments are given by

$$\begin{aligned}
\ell_1 &= \int_0^1 Q(u)\,du,\\
\ell_2 &= \int_0^1 (2u-1)Q(u)\,du,\\
\ell_3 &= \int_0^1 (6u^2-6u+1)Q(u)\,du,\\
\ell_4 &= \int_0^1 (20u^3-30u^2+12u-1)Q(u)\,du.
\end{aligned}$$

The corresponding L-moment ratios, namely the L-skewness and L-kurtosis coefficients, are defined as

$$\tau_3 = \frac{\ell_3}{\ell_2}, \qquad \tau_4 = \frac{\ell_4}{\ell_2}.$$

Substituting the quantile function $Q(u)$ of the proposed Log-LR distribution into Eq (2.13) yields the corresponding L-moments. Due to the complexity of the quantile function, the resulting integrals do not admit tractable closed-form expressions and are therefore evaluated numerically.

Table 2 shows the first four L-moments, as well as L-skewness (τ_3) and L-kurtosis (τ_4), for the three parameter settings used in the simulation study. The results show that the shape of the Log-LR distribution varies significantly with the parameters. Sets 1 and 2 have positive τ_3 values, which means they are slightly right-skewed. Set 3 ($\tau_3 = -0.1605$) is moderately left-skewed and has a longer left tail. The τ_4 values range from 0.037 to 0.179 and also differ significantly, showing differences in tail behavior and the overall shape of the distribution. These results show that the Log-LR distribution can model many types of asymmetry and tail behavior by adjusting its parameters.

Table 2. L-moments and L-moment ratios of the Log-LR distribution for selected parameter settings.

Setting	ℓ_1	ℓ_2	ℓ_3	ℓ_4	τ_3	τ_4
Set 1 $(1.5, 1.2, 1.0)$	1.1963	0.4327	0.0254	0.0283	0.0586	0.0653
Set 2 $(0.85, 0.5, 0.5)$	0.6147	0.2381	0.0099	0.0089	0.0418	0.0372
Set 3 $(0.8, 0.01, 6.0)$	16.9649	2.3176	-0.3721	0.4154	-0.1605	0.1793

2.8. *Additional properties*

2.8.1. Shannon entropy

The Shannon entropy of the Log-LR distribution is defined as

$$H_S = -E[\log g(X)] = -\int_0^\infty g(x;\boldsymbol{\omega})\, \log g(x;\boldsymbol{\omega})\, dx.$$

Using the expression of the log-density function, the entropy can be written as

$$\begin{aligned} H_S = &-\log\alpha - \alpha\log\beta + \log\lambda^2 - E[\log X] + \frac{1}{2\lambda^2}\, E[X^2] \\ &+ E\Big[\log\Big(1 - e^{-X^2/(2\lambda^2)}\Big)\Big] + (\alpha+1)\, E[\log\eta(X)]. \end{aligned}$$

The above expression follows directly from the log-density formulation of the Log-LR model. However, the expectations involved do not admit tractable closed-form expressions and are therefore evaluated numerically for given parameter values.

2.8.2. Mean residual life function

The mean residual life (MRL) function, defined as the expected remaining lifetime given survival beyond time t, is given by

$$m(t) = E[X - t \mid X > t] = \frac{1}{R(t)} \int_t^\infty R(x)\, dx,$$

where $R(x) = 1 - G(x;\boldsymbol{\omega})$ is the reliability function given in Eq (2.7). The MRL function is evaluated numerically for specific parameter configurations.

3. Order statistics

Let $X_1, X_2, \ldots, X_n$ be a random sample of size n from a continuous distribution with CDF $G_X(x)$ and PDF $g_X(x)$, and let $X_{(1)} \le X_{(2)} \le \cdots \le X_{(n)}$ denote the corresponding order statistics. The PDF of the i-th order statistic is given by [24]:

$$g_{X_{(i)}}(x) = \frac{n!}{(i-1)!\,(n-i)!}\, [G_X(x)]^{i-1}\, [1 - G_X(x)]^{n-i}\, g_X(x). \tag{3.1}$$

The PDF of the i-th order statistic takes the form

$$\begin{aligned} g_{X_{(i)}}(x) = &\frac{n!}{(i-1)!\,(n-i)!} \left[\left(\frac{\beta}{\eta(x)}\right)^{\alpha}\right]^{i-1} \left(1 - \frac{\beta}{\eta(x)}\right)^{\alpha(n-i)} \\ &\times \frac{\alpha\,\beta^\alpha\, x\, e^{-x^2/(2\lambda^2)}}{\lambda^2(1 - e^{-x^2/(2\lambda^2)})}\, [\eta(x)]^{-(\alpha+1)}. \end{aligned}$$

3.1. Smallest order statistic

Setting $i = 1$ in Eq (3.1) gives the PDF of the minimum $X_{(1)}$:

$$g_{X_{(1)}}(x) = n\, g_X(x) \left[1 - G_X(x)\right]^{n-1}.$$

For the Log-LR distribution, this yields

$$\begin{aligned} g_{X_{(1)}}(x) = {} & \frac{n\,\alpha\,\beta^{\alpha}\, x\, e^{-x^2/(2\lambda^2)}}{\lambda^2(1 - e^{-x^2/(2\lambda^2)})} \left[\eta(x)\right]^{-(\alpha+1)} \\ & \times \left[1 - \left(\frac{\beta}{\eta(x)}\right)^{\alpha}\right]^{n-1}. \end{aligned}$$

3.2. Largest order statistic

Setting $i = n$ in Eq (3.1) gives the PDF of the maximum $X_{(n)}$:

$$g_{X_{(n)}}(x) = n\, g_X(x) \left[G_X(x)\right]^{n-1}.$$

For the Log-LR distribution, this yields

$$\begin{aligned} g_{X_{(n)}}(x) = {} & \frac{n\,\alpha\,\beta^{\alpha}\, x\, e^{-x^2/(2\lambda^2)}}{\lambda^2(1 - e^{-x^2/(2\lambda^2)})} \left[\eta(x)\right]^{-(\alpha+1)} \\ & \times \left(\frac{\beta}{\eta(x)}\right)^{\alpha(n-1)}. \end{aligned}$$

4. Maximum likelihood estimation

Let $X_1, X_2, \dots, X_n$ be a random sample of size n from the Log-LR distribution with parameter vector $\boldsymbol{\omega} = (\alpha, \beta, \lambda)$. In this section, we derive the MLEs of $\boldsymbol{\omega}$ based on a complete sample.

4.1. Log-likelihood function

The likelihood function is

$$\begin{aligned} L(\boldsymbol{\omega}) &= \prod_{i=1}^{n} g(x_i;\, \boldsymbol{\omega}) \\ &= \prod_{i=1}^{n} \frac{\alpha\,\beta^{\alpha}\, x_i\, e^{-x_i^2/(2\lambda^2)}}{\lambda^2(1 - e^{-x_i^2/(2\lambda^2)})} \left[\eta_i\right]^{-(\alpha+1)}. \end{aligned}$$

The corresponding log-likelihood function is

$$\begin{aligned} \ell(\boldsymbol{\omega}) = {} & n \log\alpha + n\alpha \log\beta + \sum_{i=1}^{n} \log x_i - \frac{1}{2\lambda^2} \sum_{i=1}^{n} x_i^2 \\ & - n \log\lambda^2 - \sum_{i=1}^{n} \log\!\left(1 - e^{-x_i^2/(2\lambda^2)}\right) - (\alpha+1) \sum_{i=1}^{n} \log\eta_i. \end{aligned}$$

4.2. Score equations

The MLEs of $\boldsymbol{\omega}$ are obtained by solving the score equations $\partial\ell/\partial\alpha = 0$, $\partial\ell/\partial\beta = 0$, and $\partial\ell/\partial\lambda = 0$.

For notational convenience, let $t_i = x_i^2/(2\lambda^2)$, $F_i = 1 - e^{-t_i}$, and $w_i = e^{-t_i}/F_i$. Note that $\partial\eta_i/\partial\lambda = x_i^2\, w_i/\lambda^3$.

$$\frac{\partial\ell}{\partial\alpha} = \frac{n}{\alpha} + n\log\beta - \sum_{i=1}^{n}\log\eta_i = 0, \tag{4.1}$$

$$\frac{\partial\ell}{\partial\beta} = \frac{n\alpha}{\beta} - (\alpha+1)\sum_{i=1}^{n}\frac{1}{\eta_i} = 0, \tag{4.2}$$

$$\begin{aligned}\frac{\partial\ell}{\partial\lambda} = {} & -\frac{2n}{\lambda} + \frac{1}{\lambda^3}\sum_{i=1}^{n}x_i^2 + \frac{1}{\lambda^3}\sum_{i=1}^{n}x_i^2 w_i \\ & - \frac{\alpha+1}{\lambda^3}\sum_{i=1}^{n}\frac{x_i^2 w_i}{\eta_i}.\end{aligned} \tag{4.3}$$

The system Eqs (4.1)–(4.3) is nonlinear and has no closed-form solution. Therefore, the MLEs $\hat{\boldsymbol{\omega}} = (\hat{\alpha}, \hat{\beta}, \hat{\lambda})$ are obtained numerically by maximizing the log-likelihood function.

Regularity conditions

The standard regularity conditions relevant to maximum likelihood estimation are satisfied by the Log-LR distribution:

(1) **Parameter space:** The parameter space

$$\omega = \{(\alpha, \beta, \lambda) : \alpha > 0,\ \beta > 0,\ \lambda > 0\}$$

is an open subset of $\mathbb{R}^3$.

(2) **Identifiability:** In particular, distinct parameter vectors (α, β, λ) generate distinct distribution functions, implying a one-to-one correspondence between the parameter vector and the distribution.

(3) **Support independence:** The support $(0, \infty)$ does not depend on the model parameters.

(4) **Differentiability:** The log-likelihood function is continuous and twice continuously differentiable with respect to (α, β, λ) for all $x \in (0, \infty)$.

Under these regularity conditions, the MLEs are consistent and asymptotically normal as $n \to \infty$. Since the score equations Eqs (4.1)–(4.3) constitute a nonlinear system, closed-form solutions are unavailable. Consequently, the estimators are obtained numerically using the Limited-memory Broyden-Fletcher-Goldfarb-Shanno with Bound-constraints (L-BFGS-B) optimization algorithm. To assess the stability of the optimization procedure and reduce the possibility of convergence to local optima, multiple starting values were employed. In all simulation experiments and real-data applications considered in this study, the algorithm consistently converged to the same solution, providing empirical evidence of numerical stability.

4.3. Asymptotic properties

Under standard regularity conditions, the MLEs are asymptotically normal:

$$\sqrt{n}\,(\hat{\omega} - \omega) \xrightarrow{\mathrm{d}} N_3(\mathbf{0},\ \mathbf{I}^{-1}(\omega)),$$

where $\mathbf{I}(\omega)$ is the 3×3 Fisher information matrix with elements

$$\mathbf{I}_{jk}(\omega) = -\,\mathbb{E}\left[\frac{\partial^2 \ell}{\partial \omega_j\, \partial \omega_k}\right], \qquad j, k = 1, 2, 3.$$

The observed information matrix, obtained from the second-order partial derivatives evaluated at $\hat{\omega}$. The elements of the observed information matrix are:

$$\frac{\partial^2 \ell}{\partial \alpha^2} = -\frac{n}{\alpha^2},$$

$$\frac{\partial^2 \ell}{\partial \beta^2} = -\frac{n\alpha}{\beta^2} + (\alpha + 1) \sum_{i=1}^{n} \frac{1}{\eta_i^2},$$

$$\frac{\partial^2 \ell}{\partial \alpha\, \partial \beta} = \frac{n}{\beta} - \sum_{i=1}^{n} \frac{1}{\eta_i},$$

$$\frac{\partial^2 \ell}{\partial \alpha\, \partial \lambda} = -\frac{1}{\lambda^3} \sum_{i=1}^{n} \frac{x_i^2 w_i}{\eta_i},$$

$$\frac{\partial^2 \ell}{\partial \beta\, \partial \lambda} = \frac{(\alpha + 1)}{\lambda^3} \sum_{i=1}^{n} \frac{x_i^2 w_i}{\eta_i^2}.$$

Differentiating the score function $\partial \ell / \partial \lambda$ with respect to λ and applying the product and chain rules yields

$$\begin{aligned}\frac{\partial^2 \ell}{\partial \lambda^2} = {} & \frac{2n}{\lambda^2} - \frac{3}{\lambda^4} \sum_{i=1}^{n} x_i^2 - \frac{3}{\lambda^4} \sum_{i=1}^{n} x_i^2 w_i + \frac{1}{\lambda^6} \sum_{i=1}^{n} \frac{x_i^4 e^{-t_i}}{F_i^2} \\ & + \frac{3(\alpha + 1)}{\lambda^4} \sum_{i=1}^{n} \frac{x_i^2 w_i}{\eta_i} - \frac{(\alpha + 1)}{\lambda^6} \sum_{i=1}^{n} \frac{x_i^4 e^{-t_i}}{F_i^2 \eta_i} \\ & + \frac{(\alpha + 1)}{\lambda^6} \sum_{i=1}^{n} \frac{x_i^4 w_i^2}{\eta_i^2}.\end{aligned}$$

The score functions were obtained by direct differentiation of the log-likelihood function with respect to the model parameters (α, β, λ), using the chain rule for the composite terms. For brevity, only the resulting score equations are presented in the main text. The intermediate differentiation steps, together with the detailed derivation of the observed information matrix, are provided in Appendix B.

4.4. Confidence intervals

Approximately $100(1-\gamma)\%$ confidence intervals for each parameter ω_j are constructed as

$$\hat{\omega}_j \pm z_{\gamma/2}\sqrt{\mathbf{I}_{jj}^{-1}(\hat{\omega})},$$

where $z_{\gamma/2}$ is the upper $\gamma/2$ quantile of the standard normal distribution and $\mathbf{I}_{jj}^{-1}(\hat{\omega})$ denotes the j-th diagonal element of the inverse observed information matrix.

5. Simulation analysis

In this section, the performance of the MLEs for the Log-LR distribution is evaluated in terms of bias, mean squared error (MSE), and mean relative error (MRE). A Monte Carlo simulation study with $N = 1000$ replications was conducted for sample sizes $n = 50, 100, 200$, and 500. Three different parameter settings were considered:

- Set 1: ($\alpha = 1.5,\ \beta = 1.2,\ \lambda = 1$).
- Set 2: ($\alpha = 0.85,\ \beta = 0.5,\ \lambda = 0.5$).
- Set 3: ($\alpha = 0.8,\ \beta = 0.01,\ \lambda = 6$).

Three parameter settings were chosen to show different patterns in the Log-LR model. Set 1 ($\alpha = 1.5, \beta = 1.2, \lambda = 1$) shows a balanced setup, Set 2 ($\alpha = 0.85, \beta = 0.5, \lambda = 0.5$) represents more weight near the lower end, and Set 3 ($\alpha = 0.8, \beta = 0.01, \lambda = 6$) creates a very dispersed distribution.

Random samples were generated from the Log-LR distribution using the quantile function provided in Eq (2.9).

The MLEs were computed numerically using the L-BFGS-B algorithm implemented through the `optim()` function in R, subject to the positivity constraints $\alpha > 0, \beta > 0$, and $\lambda > 0$. To reduce the risk of convergence to local optima, multiple starting values were used for each replication, and the solution with the largest log-likelihood was retained. Standard errors were obtained from the inverse of the observed Fisher information matrix whenever the Hessian matrix was positive definite and reliably invertible. Replications for which the optimization failed to converge, or for which a valid Hessian matrix could not be obtained, were excluded from the computation of the performance measures.

The performance measures used to assess the estimators are defined as follows.

Bias

The bias of the estimators is defined by

$$\mathrm{Bias}(\hat{\alpha}) = E(\hat{\alpha}) - \alpha, \qquad \mathrm{Bias}(\hat{\beta}) = E(\hat{\beta}) - \beta, \qquad \mathrm{Bias}(\hat{\lambda}) = E(\hat{\lambda}) - \lambda.$$

Mean squared error (MSE)

The MSE of the estimators is computed as

$$\mathrm{MSE}_{\hat{\alpha}} = \frac{1}{N}\sum_{i=1}^{N}(\hat{\alpha}_i - \alpha)^2, \qquad \mathrm{MSE}_{\hat{\beta}} = \frac{1}{N}\sum_{i=1}^{N}(\hat{\beta}_i - \beta)^2, \qquad \mathrm{MSE}_{\hat{\lambda}} = \frac{1}{N}\sum_{i=1}^{N}(\hat{\lambda}_i - \lambda)^2.$$

Mean relative error (MRE)

The MRE is defined as

$$\mathrm{MRE}_{\hat{\alpha}} = \frac{1}{N}\sum_{i=1}^{N}\frac{|\hat{\alpha}_i - \alpha|}{\alpha}, \qquad \mathrm{MRE}_{\hat{\beta}} = \frac{1}{N}\sum_{i=1}^{N}\frac{|\hat{\beta}_i - \beta|}{\beta}, \qquad \mathrm{MRE}_{\hat{\lambda}} = \frac{1}{N}\sum_{i=1}^{N}\frac{|\hat{\lambda}_i - \lambda|}{\lambda}.$$

Besides bias, MSE, and MRE, two measures related to confidence intervals were also considered:

- **Coverage probability (CP):** the proportion of Monte Carlo replications for which the nominal (95%) asymptotic confidence interval

$$\hat{\omega}_j \pm z_{0.025}\sqrt{\mathbf{I}^{-1}_{jj}(\hat{\omega})}$$

  contains the true parameter value (ω_j), where $\mathbf{I}^{-1}_{jj}(\hat{\omega})$ denotes the j-th diagonal element of the inverse observed Fisher information matrix.
- **Average length (AL):** the average size of the (95%) confidence intervals across all replications, calculated as

$$\mathrm{AL} = \frac{1}{N}\sum_{i=1}^{N} 2z_{0.025}\,\mathrm{SE}_i(\hat{\omega}_j),$$

  where $\mathrm{SE}_i(\hat{\omega}_j)$ is the estimated standard error of $\hat{\omega}_j$ in the i-th replication.

A good estimation method should yield coverage probabilities near 0.95, and the average interval length should decrease as the sample size grows.

Overall, the simulation results reported in Tables 3–5 demonstrate that the MLEs perform satisfactorily, as the bias, MSE, and MRE values decrease consistently with increasing sample size, confirming the consistency of the estimators. As the sample size n increases, the coverage probabilities for $\hat{\alpha}$ reach the nominal 95% level across all three parameter settings. In contrast, the coverage probabilities for $\hat{\lambda}$ stay below the expected level and often do not improve much as n grows. This suggests that the observed Fisher information matrix tends to underestimate the extent of variation in $\hat{\lambda}$, leading to confidence intervals that are too narrow. A similar trend is seen for $\hat{\beta}$ in Parameter Set 2. This problem often happens with Wald-type confidence intervals, especially for scale and shape parameters in complex or heavy-tailed models. In these cases, the normal approximation is less accurate, and the likelihood surface can cause variance estimates to be off when the sample size is small.

Table 3. Performance of MLE estimators for $\alpha = 1.5, \beta = 1.2$, and $\lambda = 1$.

n	Bias			MSE			MRE			CP			AL		
	α	β	λ	α	β	λ	α	β	λ	α	β	λ	α	β	λ
50	0.28773	0.42080	-0.01296	0.68780	1.50713	0.01337	0.38122	0.72694	0.09357	0.94145	0.89093	0.79793	3.95412	5.79793	0.39441
100	0.23611	0.33041	0.00071	0.42703	0.91103	0.00638	0.29089	0.54031	0.06430	0.96383	0.92553	0.76596	2.46229	3.57480	0.25913
200	0.15827	0.22598	0.00368	0.17528	0.41229	0.00371	0.19710	0.37671	0.04897	0.97056	0.93691	0.70032	1.49489	2.14718	0.16852
500	0.11296	0.15481	0.00410	0.06425	0.13912	0.00132	0.12571	0.22923	0.02955	0.96519	0.94831	0.64346	0.85998	1.20330	0.09557

Table 4. Performance of MLE estimators for $\alpha = 0.85, \beta = 0.5$, and $\lambda = 0.5$.

n	Bias			MSE			MRE			CP			AL		
	α	β	λ	α	β	λ	α	β	λ	α	β	λ	α	β	λ
50	0.18693	0.23844	-0.00213	0.14970	0.30720	0.00340	0.31785	0.79166	0.09420	0.96954	0.88706	0.47716	1.46027	1.97496	0.11793
100	0.18027	0.24234	0.00833	0.09376	0.21947	0.00196	0.26019	0.65341	0.06993	0.98418	0.94404	0.41484	0.95996	1.30409	0.07537
200	0.15358	0.18529	0.00692	0.05093	0.10434	0.00100	0.20513	0.47913	0.05065	0.93443	0.88407	0.37471	0.62897	0.80814	0.04754
500	0.13351	0.16291	0.00786	0.03549	0.07850	0.00062	0.16663	0.37987	0.03937	0.75897	0.73077	0.34487	0.37997	0.48363	0.02673

Table 5. Performance of MLE estimators for $\alpha = 0.8, \beta = 0.01$, and $\lambda = 6$.

n	Bias			MSE			MRE			CP			AL		
	α	β	λ	α	β	λ	α	β	λ	α	β	λ	α	β	λ
50	0.07797	0.00352	-0.03078	0.07517	0.00014	0.14106	0.24196	0.83366	0.05174	0.95169	0.77536	0.87077	1.25264	0.06480	1.70460
100	0.07507	0.00419	0.03559	0.05024	0.00013	0.09714	0.20674	0.78388	0.04283	0.96000	0.85730	0.89946	0.87908	0.04745	1.27117
200	0.07602	0.00417	0.06492	0.03327	0.00009	0.06368	0.16668	0.65722	0.03362	0.96859	0.90681	0.91518	0.62355	0.03318	0.93223
500	0.04757	0.00269	0.06433	0.01115	0.00003	0.03074	0.09689	0.40173	0.02320	0.96548	0.91946	0.86506	0.36671	0.01803	0.58255

6. Real data applications

In this section, the practical applicability of the proposed Log-LR distribution is demonstrated through four real datasets from different domains. To assess the relative performance of the Log-LR model, nine competing distributions are considered: the Rayleigh (Ray), Weibull (Weib), Gamma, Lomax, logistic Lomax (LL), logistic inverse Lomax (LIL), Generalized inverse Rayleigh (GIR), Gumbel–Lomax (GL), and Alpha power Lomax (APL). The CDF and PDF of each competing distribution are summarized below.

The CDF and PDF of the Rayleigh distribution are given in Eqs (2.3) and (2.4), respectively.

The CDF and PDF of the Weibull distribution are given by

$$F_{\mathrm{W}}(x;\alpha,\lambda) = 1 - \exp\!\left(-\left(\frac{x}{\lambda}\right)^{\alpha}\right), \qquad x > 0,\ \alpha,\lambda > 0,$$

$$f_{\mathrm{W}}(x;\alpha,\lambda) = \frac{\alpha}{\lambda}\left(\frac{x}{\lambda}\right)^{\alpha-1}\exp\!\left(-\left(\frac{x}{\lambda}\right)^{\alpha}\right).$$

The CDF and PDF of the Gamma distribution are given by

$$F_{\mathrm{Ga}}(x;\alpha,\lambda) = \frac{\gamma(\alpha,\ x/\lambda)}{\Gamma(\alpha)}, \qquad x > 0,\ \alpha,\lambda > 0,$$

$$f_{\mathrm{Ga}}(x;\alpha,\lambda) = \frac{x^{\alpha-1}\exp(-x/\lambda)}{\lambda^{\alpha}\,\Gamma(\alpha)},$$

where $\gamma(\cdot,\cdot)$ denotes the lower incomplete Gamma function and $\Gamma(\cdot)$ is the Gamma function.

The CDF and PDF of the Lomax distribution are given by

$$F_{\mathrm{Lx}}(x;\alpha,\lambda) = 1 - \left(1 + \frac{x}{\lambda}\right)^{-\alpha}, \qquad x > 0,\ \alpha,\lambda > 0,$$

$$f_{\mathrm{Lx}}(x;\alpha,\lambda) = \frac{\alpha}{\lambda}\left(1 + \frac{x}{\lambda}\right)^{-(\alpha+1)}.$$

The CDF and PDF of the LL distribution are given in [25] as

$$F_{\mathrm{LL}}(x;\alpha,\beta,\lambda) = \frac{\left[(1+\lambda x)^{\beta} - 1\right]^{\alpha}}{1 + \left[(1+\lambda x)^{\beta} - 1\right]^{\alpha}}, \qquad x > 0,\ \alpha,\beta,\lambda > 0,$$

$$f_{\mathrm{LL}}(x;\alpha,\beta,\lambda) = \frac{\alpha\beta\lambda(1+\lambda x)^{\beta-1}\left[(1+\lambda x)^{\beta} - 1\right]^{\alpha-1}}{\{1 + [(1+\lambda x)^{\beta} - 1]^{\alpha}\}^{2}}.$$

The CDF and PDF of the LIL distribution are given in [26] as

$$F_{\mathrm{LIL}}(x;\alpha,\beta,\lambda)=\frac{\left[\left(1+\frac{\lambda}{x}\right)^{\beta}-1\right]^{\alpha}}{1+\left[\left(1+\frac{\lambda}{x}\right)^{\beta}-1\right]^{\alpha}},\qquad x>0,\ \alpha,\beta,\lambda>0,$$

$$f_{\mathrm{LIL}}(x;\alpha,\beta,\lambda)=\frac{\alpha\lambda\beta\,x^{-2}\left(1+\frac{\lambda}{x}\right)^{\beta-1}\left[\left(1+\frac{\lambda}{x}\right)^{\beta}-1\right]^{\alpha-1}}{\left\{1+\left[\left(1+\frac{\lambda}{x}\right)^{\beta}-1\right]^{\alpha}\right\}^{2}}.$$

The CDF and PDF of the GIR distribution are given in [27] as

$$F_{\mathrm{GIR}}(x;\alpha,\lambda)=1-\left[1-\exp\left(-\frac{\lambda}{x^{2}}\right)\right]^{\alpha},\qquad x>0,\ \alpha,\lambda>0,$$

$$f_{\mathrm{GIR}}(x;\alpha,\lambda)=\frac{2\alpha\lambda}{x^{3}}\,\exp\left(-\frac{\lambda}{x^{2}}\right)\left[1-\exp\left(-\frac{\lambda}{x^{2}}\right)\right]^{\alpha-1}.$$

The CDF and PDF of the GL distribution are given in [19] as

$$F_{\mathrm{GL}}(x;\alpha,\beta,\lambda,\sigma)=1-\exp\left(-\exp\left(\frac{F_{\mathrm{Lx}}(x;\alpha,\beta)-\lambda}{\sigma}\right)\right),\qquad x>0,\ \alpha,\ \beta>0,\ \lambda\in\mathbb{R},\ \sigma>0,$$

$$f_{\mathrm{GL}}(x;\alpha,\beta,\lambda,\sigma)=\frac{f_{\mathrm{Lx}}(x;\alpha,\beta)}{\sigma}\,\exp\left(\frac{F_{\mathrm{Lx}}(x)-\lambda}{\sigma}-\exp\left(\frac{F_{\mathrm{Lx}}(x)-\lambda}{\sigma}\right)\right),$$

where F_{Lx} and f_{Lx} denote the CDF and PDF of the Lomax distribution, respectively.

The CDF and PDF of the Alpha Power Lomax (APL) distribution are given in [20] as:

$$F_{\mathrm{APL}}(x;\alpha,\beta,\lambda)=\frac{\alpha^{F_{\mathrm{Lx}}(x;\beta,\lambda)}-1}{\alpha-1},\qquad x>0,\ \alpha>0,\ \alpha\neq1,\ \beta,\lambda>0,$$

$$f_{\mathrm{APL}}(x;\alpha,\beta,\lambda)=\frac{\log\alpha}{\alpha-1}\,f_{\mathrm{Lx}}(x;\beta,\lambda)\,\alpha^{F_{\mathrm{Lx}}(x;\beta,\lambda)},$$

where F_{Lx} and f_{Lx} denote the CDF and PDF of the Lomax distribution, respectively.

The Total Time on Test (TTT) plots for the four datasets, shown in Figure 5, exhibit concave shapes that lie above the diagonal line, indicating decreasing failure rates. This empirical evidence supports the use of the Log-LR distribution, which features a monotonically decreasing HRF, as an appropriate model to fit these datasets. The Log-LR model is compared against nine competing distributions, as detailed below.

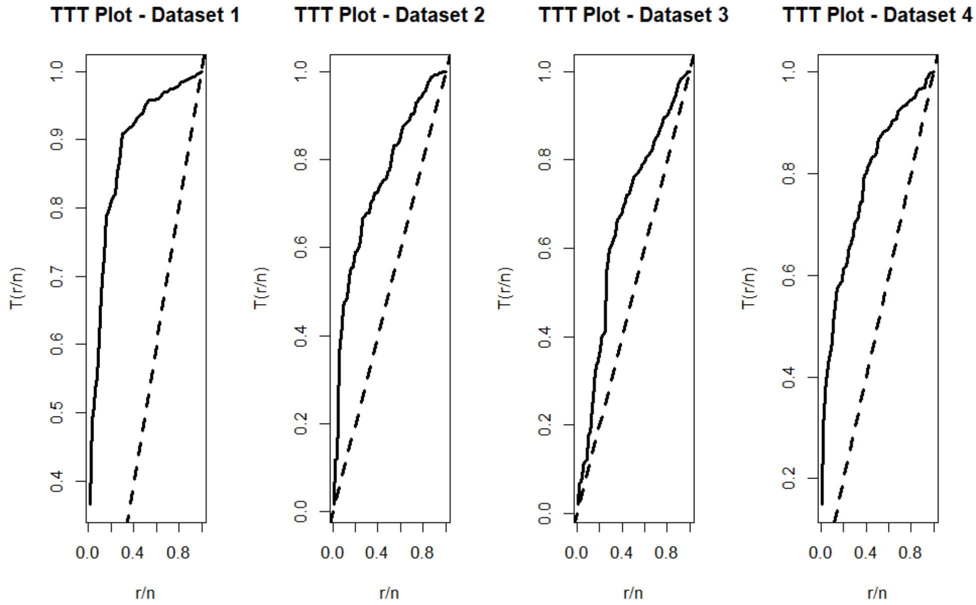

Figure 5. TTT plots for the four datasets.

The following goodness-of-fit statistics are used to compare the competing models: the Kolmogorov–Smirnov (KS) statistic, which measures the maximum absolute difference between the empirical and fitted CDFs; the Anderson–Darling (AD) statistic, which places greater weight on the tails; and the Cramér–von Mises (CvM) statistic, which measures the integrated squared difference. Smaller values of KS, AD, and CvM indicate a better fit. The associated p-values are also reported; larger p-values indicate stronger evidence in favor of the fitted model.

6.1. Dataset 1: Glass fiber strengths

The first dataset, obtained from [27], represents the strengths of 1.5 cm glass fibers measured at the National Physical Laboratory in England. The dataset consists of $n = 63$ observations:

0.55, 0.93, 1.25, 1.36, 1.49, 1.52, 1.58, 1.61, 1.64, 1.68, 1.73, 1.81, 2.00, 0.74, 1.04, 1.27, 1.39, 1.49, 1.53, 1.59, 1.61, 1.66, 1.68, 1.76, 1.82, 2.01, 0.77, 1.11, 1.28, 1.42, 1.50, 1.54, 1.60, 1.62, 1.66, 1.69, 1.76, 1.84, 2.24, 0.81, 1.13, 1.29, 1.48, 1.50, 1.55, 1.61, 1.62, 1.66, 1.70, 1.77, 1.84, 0.84, 1.24, 1.30, 1.48, 1.51, 1.55, 1.61, 1.63, 1.67, 1.70, 1.78, 1.89.

The summary statistics are presented in Table 6, and the MLEs and standard errors (SEs) for all fitted distributions are reported in Table 7.

Table 6. Summary statistics for Dataset 1.

Min.	1st Qu.	Median	Mean	3rd Qu.	Max.
0.550	1.375	1.590	1.507	1.685	2.240

Table 7. MLEs and SEs (in parentheses) for the fitted distributions for Dataset 1.

Distribution	Estimates (SE)
Ray	$\hat{\lambda}$ = 1.0895 (0.0686)
Weib	$\hat{\alpha}$ = 5.7807 (0.5761), $\hat{\lambda}$ = 1.6281 (0.0371)
Gamma	$\hat{\alpha}$ = 17.4396 (3.0780), $\hat{\lambda}$ = 11.5737 (2.0723)
Lomax	$\hat{\alpha}$ = 27804.57 (3502.92), $\hat{\lambda}$ = 41907.50 (285.39)
LL	$\hat{\alpha}$ = 6.1155 (0.7018), $\hat{\beta}$ = 0.0522 (0.0388), $\hat{\lambda}$ = 9.0342 (6.4582)
LIL	$\hat{\alpha}$ = 13.9330 (2.7735), $\hat{\beta}$ = 9.9485 (5.3822), $\hat{\lambda}$ = 0.3438 (0.0799)
GIR	$\hat{\alpha}$ = 4.5150 (0.6172), $\hat{\lambda}$ = 5.7974 (1.6301)
GL	$\hat{\alpha}$ = 3.5089 (15.0821), $\hat{\beta}$ = 11.1804 (44.7453), $\hat{\lambda}$ = 0.3814 (0.3093), $\hat{\sigma}$ = 0.0460 (0.0319)
APL	$\hat{\alpha}$ = 100.00 (41.41), $\hat{\beta}$ = 50.00 (33.16), $\hat{\lambda}$ = 34.49 (23.40)
LogLR	$\hat{\alpha}$ = 0.7983 (0.1498), $\hat{\beta}$ = 0.0039 (0.0018), $\hat{\lambda}$ = 0.4808 (0.0178)

As presented in Table 7, the fitted Log-LR parameters $(\hat{\alpha}, \hat{\beta}, \hat{\lambda}) = (0.798,\ 0.004,\ 0.481)$ provide insight into the distributional characteristics of the glass fiber strength data. The estimate $\hat{\alpha} = 0.798$ indicates a moderate shape effect through the term $\eta(x)^{-(\alpha+1)}$, influencing the curvature of both the density and HRFs. It does not, by itself, imply a monotone-decreasing hazard structure; rather, it controls the degree of deviation from exponential-type behavior. The very small estimate $\hat{\beta} \approx 0.004$ suggests that the transformation $\eta(x) = \beta - \log(1 - e^{-x^2/(2\lambda^2)})$ is dominated by the logarithmic term over most of the support, which affects the allocation of probability mass but does not directly determine the mode's location. Finally, the scale parameter $\hat{\lambda} = 0.481$ governs the overall scale of the distribution and reflects the characteristic magnitude of the observed strength measurements.

6.2. Dataset 2: Aircraft windshield failure times

The second dataset, obtained from [28], represents $n = 84$ recorded failure times of aircraft windshields:

0.040, 1.866, 2.385, 3.443, 0.301, 1.876, 2.481, 3.467, 0.309, 1.899, 2.610, 3.478, 0.557, 1.911, 2.625, 3.578, 0.943, 1.912, 2.632, 3.595, 1.070, 1.914, 2.646, 3.699, 1.124, 1.981, 2.661, 3.779, 1.248, 2.010, 2.688, 3.924, 1.281, 2.038, 2.823, 4.035, 1.281, 2.085, 2.890, 4.121, 1.303, 2.089, 2.902, 4.167, 1.432, 2.097, 2.934, 4.240, 1.480, 2.135, 2.962, 4.255, 1.505, 2.154, 2.964, 4.278, 1.506, 2.190, 3.000, 4.305, 1.568, 2.194, 3.103, 4.376, 1.615, 2.223, 3.114, 4.449, 1.619, 2.224, 3.117, 4.485, 1.652, 2.229, 3.166, 4.570, 1.652, 2.300, 3.344, 4.602, 1.757, 2.324, 3.376, 4.663.

The summary statistics are presented in Table 8, and the MLEs and SEs are reported in Table 9.

As presented in Table 9, the fitted parameter estimates $(\hat{\alpha}, \hat{\beta}, \hat{\lambda}) = (2.979,\ 1.360,\ 1.627)$ suggest a flexible and moderately dispersed distribution. The estimates of α and β jointly determine the distributional shape and hazard-rate behavior, whereas λ controls the overall time scale. In particular, $\hat{\lambda} = 1.627$ corresponds to the characteristic failure-time range (measured in units of 10^3 hours) for the windshield data.

Table 8. Summary statistics for Dataset 2.

Min.	1st Qu.	Median	Mean	3rd Qu.	Max.
0.040	1.839	2.354	2.557	3.393	4.663

Table 9. MLEs and SEs (in parentheses) for the fitted distributions for Dataset 2.

Distribution	Estimates (SE)
Ray	$\hat{\lambda}$ = 1.9720 (0.1076)
Weib	$\hat{\alpha}$ = 2.3744 (0.2096), $\hat{\lambda}$ = 2.8629 (0.1375)
Gamma	$\hat{\alpha}$ = 3.4923 (0.5152), $\hat{\lambda}$ = 1.3655 (0.2167)
Lomax	$\hat{\alpha}$ = 57874.40 (6849.90), $\hat{\lambda}$ = 148009.80 (558.67)
LL	$\hat{\alpha}$ = 2.4534 (0.2335), $\hat{\beta}$ = 0.0190 (0.0120), $\hat{\lambda}$ = 15.5400 (9.6582)
LIL	$\hat{\alpha}$ = 6.6734 (2.3987), $\hat{\beta}$ = 27.8971 (34.2789), $\hat{\lambda}$ = 0.2738 (0.1222)
GIR	$\hat{\alpha}$ = 0.0257 (0.0069), $\hat{\lambda}$ = 0.1894 (0.0227)
GL	$\hat{\alpha}$ = 0.1278 (0.1765), $\hat{\beta}$ = 0.9040 (0.9466), $\hat{\mu}$ = 0.1685 (0.1823), $\hat{\sigma}$ = 0.0313 (0.0332)
APL	$\hat{\alpha}$ = 100.00 (50.11), $\hat{a}$ = 42.6425 (30.3511), $\hat{b}$ = 50.00 (36.56)
Log-LR	$\hat{\alpha}$ = 2.9787 (1.5602), $\hat{\beta}$ = 1.3598 (1.0668), $\hat{\lambda}$ = 1.6270 (0.1250)

6.3. Dataset 3

The third dataset comprises failure-time observations commonly used in reliability studies and is adapted from the lifetime data reported in [29]. The dataset consists of $n = 97$ observations:

0.0251, 0.0886, 0.0891, 0.1070, 0.1449, 0.1553, 0.1557, 0.1613, 0.1630, 0.2433, 0.2570, 0.2813, 0.3535, 0.3585, 0.4333, 0.4566, 0.4902, 0.5043, 0.5355, 0.5376, 0.5862, 0.6023, 0.6191, 0.6, 0.8580, 0.8725, 0.9121, 0.9451, 0.9566, 0.9607, 0.9850, 0.9986, 1.0028, 1.0558, 1.0774, 1.0818, 1.0930, 1.1005, 1.1208, 1.1468, 1.1533, 1.1740, 1.2043, 1.2085, 1.2171, 1.2410, 1.2558, 1.2752, 1.3103, 1.3126, 1.3223, 1.3303, 1.3452, 1.3502, 1.3576, 1.3862, 1.4015, 1.4078, 1.4335, 1.4519, 1.4547, 1.4610, 1.4730, 1.5043, 1.5242, 1.5748, 1.5941, 1.6147, 1.6228, 1.6408, 1.7034, 1.7304, 1.7455, 1.8068, 1.8452, 1.8563, 1.8702, 1.8879, 1.9522, 1.9703, 1.9843, 2.0937, 2.1015, 2.2199, 2.2586, 2.3880, 2.4980, 2.5749, 2.6553, 2.7369, 2.7405, 2.8001, 2.8925, 2.9271, 3.1450, 3.2758, 3.3321.

The summary statistics are presented in Table 10, and the MLEs and SEs are reported in Table 11.

Table 10. Summary statistics for Dataset 3.

Min.	1st Qu.	Median	Mean	3rd Qu.	Max.
0.0251	0.8580	1.3103	1.3269	1.7455	3.3321

Table 11. MLEs and SEs of model parameters for Dataset 3.

Distribution	Parameter estimates (SE)
Ray	$\hat{\lambda}$ = 1.0935 (0.0555)
Weib	$\hat{\alpha}$ = 1.614 (0.1343), $\hat{\lambda}$ = 1.4694 (0.0966)
Gamma	$\hat{\alpha}$ = 1.891 (0.2513), $\hat{\lambda}$ = 1.4251 (0.2166)
Lomax	$\hat{\alpha}$ = 53297.02 (5060.858), $\hat{\lambda}$ = 70717.68 (260.2712)
LL	$\hat{\alpha}$ = 1.5967 (0.1489), $\hat{\beta}$ = 0.0157 (0.0113), $\hat{\lambda}$ = 38.9844 (27.9202)
LIL	$\hat{\alpha}$ = 4.5233 (1.3769), $\hat{\beta}$ = 14.2539 (14.8488), $\hat{\lambda}$ = 0.2686 (0.1001)
GIR	$\hat{\alpha}$ = 0.0257 (0.0069), $\hat{\lambda}$ = 0.1894 (0.0227)
GL	$\hat{\alpha}$ = 0.0398 (*NA*), $\hat{\beta}$ = 0.1829 (*NA*), $\hat{\lambda}$ = 0.0849) (*NA*), $\hat{\sigma}$ = 0.0186 (*NA*)
APL	$\hat{\alpha}$ = 28.0647 (18.1892), $\hat{\beta}$ = 50 (51.1545), $\hat{\lambda}$ = 35.5722 (37.6632)
LogLR	$\hat{\alpha}$ = 4.6544 (3.8367), $\hat{\beta}$ = 5.01 (5.3451), $\hat{\lambda}$ = 1.1433 (0.1044)

As presented in Table 11, the fitted parameter estimates $(\hat{\alpha}, \hat{\beta}, \hat{\lambda}) = (4.654,\ 5.010,\ 1.143)$ suggest a relatively smooth distributional shape. The estimates of α and β jointly determine the overall shape of the fitted distribution, while the relatively large SEs for these parameters (3.84 and 5.35, respectively) indicate substantial uncertainty in their estimates. This suggests that the data provide only limited information about the finer features of the distributional shape. In contrast, the scale parameter $\hat{\lambda}$ = 1.143 is estimated with considerably greater precision (SE = 0.104), indicating a stable estimate of the characteristic scale of the failure-time distribution.

6.4. Dataset 4: the breaking stresses of carbon fibers

The fourth dataset, obtained from [30, 31], gives the breaking stresses of single carbon fibers with a length of 50 mm, consisting of $n = 100$ observations: 3.70, 2.74, 2.73, 2.50, 3.60, 3.11, 3.27, 2.87, 1.47, 3.11, 4.42, 2.41, 3.19, 3.22, 1.69, 3.28, 3.09, 1.87, 3.15, 4.90, 3.75, 2.43, 2.95, 2.97, 3.39, 2.96, 2.53, 2.67, 2.93, 3.22, 3.39, 2.81, 4.20, 3.33, 2.55, 3.31, 3.31, 2.85, 2.56, 3.56, 3.15, 2.35, 2.55, 2.59, 2.38, 2.81, 2.77, 2.17, 2.83, 1.92, 1.41, 3.68, 2.97, 1.36, 0.98, 2.76, 4.91, 3.68, 1.84, 1.59, 3.19, 1.57, 0.81, 5.56, 1.73, 1.59, 2.00, 1.22, 1.12, 1.71, 2.17, 1.17, 5.08, 2.48, 1.18, 3.51, 2.17, 1.69, 1.25, 4.38, 1.84, 0.39, 3.68, 2.48, 0.85, 1.61, 2.79, 4.70, 2.03, 1.80, 1.57, 1.08, 2.03, 1.61, 2.12, 1.89, 2.88, 2.82, 2.05, 3.65.

The summary statistics are presented in Table 12; MLEs and SEs are reported in Table 13.

Table 12. Summary statistics for Dataset 4.

Min.	1st Qu.	Median	Mean	3rd Qu.	Max.
0.390	1.840	2.700	2.621	3.220	5.560

Table 13. MLEs and SEs of model parameters for Dataset 4.

Distribution	Parameter estimates (SE)
Ray	$\hat{\lambda}$ = 1.9861 (0.0993)
Weib	$\hat{\alpha}$ = 2.7929 (0.2141), $\hat{\lambda}$ = 2.9437 (0.1111)
Gamma	$\hat{\alpha}$ = 5.9526 (0.8193), $\hat{\lambda}$ = 2.2708 (0.3261)
Lomax	$\hat{\lambda}$ = 662533.2 (NA), $\hat{\lambda}$ = 1737168 (NA)
LL	$\hat{\alpha}$ = 3.1204 (0.2767), $\hat{\beta}$ = 0.0286 (0.0201), $\hat{\lambda}$ = 9.9823 (6.7908)
LIL	$\hat{\alpha}$ = 8.4553 (4.2827), $\hat{\beta}$ = 30.8516 (54.7632), $\hat{\lambda}$ = 0.2681 (0.1702)
GIR	$\hat{\alpha}$ = 3.5849 (0.4907), $\hat{\lambda}$ = 1.1397 (0.1656)
GL	$\hat{\alpha}$ = 0.3702 (1.0384), $\hat{\beta}$ = 0.4493 (1.9476), $\hat{\lambda}$ = 0.5252 (0.3794), $\hat{\sigma}$ = 0.0544 (0.0803)
APL	$\hat{\alpha}$ = 100.0000 (38.7228), $\hat{\beta}$ = 42.1214 (25.0557), $\hat{\lambda}$ = 50.0000 (30.4944)
LogLR	$\hat{\alpha}$ = 9.5281 (14.5325), $\hat{\beta}$ = 4.3388 (7.7791), $\hat{\lambda}$ = 1.6004 (0.1214)

As presented in Table 13, the fitted parameter estimates $(\hat{\alpha}, \hat{\beta}, \hat{\lambda}) = (9.528,\ 4.339,\ 1.600)$ suggest a relatively smooth distributional shape with moderate dispersion. The shape parameters α and β jointly govern the overall form of the fitted distribution and its associated hazard-rate behavior. However, the relatively large SEs associated with these estimates, SE($\hat{\alpha}$) = 14.53 and SE($\hat{\beta}$) = 7.78, indicate substantial uncertainty in estimating the shape parameters. This suggests that the data provide limited information about the finer aspects of the distributional shape and that the likelihood surface may be relatively flat in certain directions. Such behavior is not uncommon in flexible lifetime models and may partly reflect the moderate sample size. In contrast, the scale parameter $\hat{\lambda} = 1.600$ is estimated with considerably greater precision (SE = 0.121), indicating a stable estimate of the characteristic breaking-stress level.

6.5. Discussion

For the first dataset, as presented in Tables 14 and 15, the Log-LR model achieves the lowest AIC, BIC, KS, AD, and CvM values and the highest log-likelihood among all competing distributions, with all p-values well above the significance level of 0.05, indicating an excellent overall fit. For the second dataset, as presented in Table 16, the Log-LR model again yields the lowest AIC and BIC values and the highest log-likelihood. As shown in Table 17, the Weibull distribution yields marginally lower KS and CvM statistics, but all p-values for the Log-LR model remain comfortably above the 0.05 threshold, confirming the fit's suitability. For the third dataset, as presented in Tables 18 and 19, the Log-LR model once again outperforms all competing distributions across every goodness-of-fit criterion, further demonstrating its robustness. From Tables 20 and 21, strong competition is observed among the Log-LR, Weibull, Gamma, and GL distributions. Although the Weibull model yields slightly smaller AIC and BIC values owing to its simpler two-parameter structure, the Log-LR distribution achieves a higher log-likelihood and a larger AD p-value, indicating that both models provide excellent fits, with the Log-LR model offering greater flexibility at the expense of additional parameters. The PDFs, CDFs, Quantile-Quantile (QQ) plots, and Probability-Probability (PP) plots shown in Figures 6–21 further support the numerical findings. The graphical results suggest that the Log-LR model fits all four datasets well. The fitted densities follow the main patterns of the data, including skewness, peakedness, and tail behavior. The empirical CDFs are close to the fitted CDFs across all observations. The PP and QQ plots also show points near the 45° line. These results agree with the numerical goodness-of-fit measures and support the use of the Log-LR model.

Table 14. Model selection criteria for the fitted distributions for Dataset 1.

Distribution	LogLik	AIC	BIC
Ray	-49.7909	101.5818	103.7249
Weib	-15.2068	34.4137	38.7000
Gamma	-23.9515	51.9031	56.1893
Lomax	-88.8314	181.6628	185.9491
LL	-20.7574	47.5148	53.9442
LIL	-21.3944	48.7889	55.2183
GIR	-33.6669	71.3338	75.6201
GL	-14.2320	36.4640	45.0366
APL	-55.4905	116.9810	123.4104
LogLR	-12.5729	31.1459	37.5753

Table 15. Goodness-of-fit statistics for the fitted distributions for Dataset 1.

Distribution	KS	p-value	AD	p-value	CVM	p-value
Ray	0.3339	0.0000	11.4249	0.0000	2.3221	0.0000
Weib	0.1522	0.1078	1.2407	0.2524	0.2151	0.2403
Gamma	0.2164	0.0055	3.0873	0.0249	0.5659	0.0269
Lomax	0.4179	0.0000	18.4199	0.0000	3.8607	0.0000
LL	0.1494	0.1201	2.0771	0.0835	0.2724	0.1620
LIL	0.1487	0.1231	2.1568	0.0756	0.2705	0.1641
GIR	0.9474	0.0000	∞	0.0000	20.3964	0.0000
GL	0.1346	0.2039	0.9084	0.4087	0.1621	0.3553
APL	0.3065	0.0000	10.7093	0.0000	2.0887	0.0000
LogLR	0.1032	0.5128	0.5351	0.7106	0.0885	0.6458

Table 16. Model selection criteria for competing distributions for Dataset 2.

Distribution	LogLik	AIC	BIC
Ray	-131.7978	265.5957	268.0265
Weib	-130.0533	264.1067	268.9683
Gamma	-136.9368	277.8737	282.7353
Lomax	-162.8776	329.7551	334.6168
LL	-134.2244	274.4488	281.7412
LIL	-135.1076	276.2153	283.5077
GIR	-245.6525	495.3050	500.1667
GL	-127.5578	263.1156	272.8388
APL	-134.8667	275.7333	283.0258
LogLR	-127.3176	260.6352	267.9276

Table 17. Goodness-of-fit tests for competing distributions for Dataset 2.

Distribution	KS.D	KS_p	AD.An	AD_p	CVM.ω^2	CVM_p
Ray	0.1109	0.2528	1.4379	0.1920	0.2182	0.2351
Weib	0.0537	0.9689	0.5603	0.6858	0.0512	0.8700
Gamma	0.1034	0.3299	1.3793	0.2081	0.1716	0.3304
Lomax	0.3028	0.0000	11.5423	0.0000	2.3054	0.0000
LL	0.0777	0.6916	0.7255	0.5375	0.0537	0.8549
LIL	0.0865	0.5553	0.7714	0.5017	0.0508	0.8729
GIR	0.6970	0.0000	62.7869	0.0000	13.1026	0.0000
GL	0.0821	0.6224	0.5059	0.7403	0.0710	0.7467
APL	0.1246	0.1473	2.0533	0.0860	0.3094	0.1271
LogLR	0.0804	0.6497	0.5158	0.7303	0.0701	0.7524

Table 18. Model selection criteria for competing distributions for Dataset 3.

Distribution	LogLik	AIC	BIC
Ray	-114.7451	231.4903	234.0650
Weib	-111.0657	226.1315	231.2809
Gamma	-114.7283	233.4565	238.6059
Lomax	-124.4383	252.8766	258.0261
LL	-114.8766	235.7532	243.4773
LIL	-117.8891	241.7782	249.5023
GIR	-245.6525	495.3050	500.4544
GL	-110.7502	229.5004	239.7993
APL	-111.7227	229.4454	237.1695
LogLR	-108.4248	222.8496	230.5738

Table 19. Goodness-of-fit statistics for competing distributions for Dataset 3.

Distribution	KS.D	KS_p	AD.An	AD_p	CVM.ω^2	CVM_p
Ray	0.0993	0.2754	2.3648	0.0585	0.1570	0.3694
Weib	0.1093	0.1825	1.2916	0.2350	0.2146	0.2411
Gamma	0.1459	0.0289	2.0976	0.0814	0.4017	0.0713
Lomax	0.2311	0.0000	6.0012	0.0010	1.2351	0.0007
LL	0.1208	0.1083	1.8033	0.1183	0.2907	0.1436
LIL	0.1072	0.2000	2.1230	0.0788	0.2760	0.1582
GIR	0.5129	0.0000	43.7916	0.0000	9.4490	0.0000
GL	0.0816	0.5112	0.7687	0.5038	0.1213	0.4908
APL	0.1068	0.2032	1.1975	0.2684	0.2087	0.2514
LogLR	0.0789	0.5543	0.5996	0.6479	0.1039	0.5669

Table 20. Model selection criteria for competing distributions for Dataset 4.

Distribution	LogLik	AIC	BIC
Ray	-149.5009	301.0018	303.6070
Weib	-141.5293	287.0586	292.2689
Gamma	-143.2336	290.4673	295.6776
Lomax	-196.3709	396.7418	401.9522
LL	-143.6095	293.2191	301.0346
LIL	-144.4354	294.8708	302.6863
GIR	-174.8407	353.6813	358.8917
GL	-141.3396	290.6792	301.0999
APL	-155.5856	317.1711	324.9866
LogLR	-141.3270	288.6540	296.4695

Table 21. Goodness-of-fit statistics for competing distributions for Dataset 4.

Distribution	KS.D	KS_p	AD.An	AD_p	CVM.ω^2	CVM_p
Ray	0.1383	0.0435	3.5460	0.0146	0.6340	0.0183
Weib	0.0605	0.8578	0.4177	0.8307	0.0633	0.7942
Gamma	0.0934	0.3471	0.7589	0.5113	0.1502	0.3896
Lomax	0.3205	0.0000	17.2960	0.0000	3.4324	0.0000
LL	0.0854	0.4599	0.7538	0.5152	0.1292	0.4602
LIL	0.0857	0.4544	0.8642	0.4367	0.1396	0.4234
GIR	0.4781	0.0000	Inf	0.0000	10.2662	0.0000
GL	0.0656	0.7819	0.4052	0.8422	0.0701	0.7518
APL	0.1487	0.0241	4.6056	0.0045	0.7832	0.0079
LogLR	0.0675	0.7523	0.4067	0.8428	0.0720	0.7404

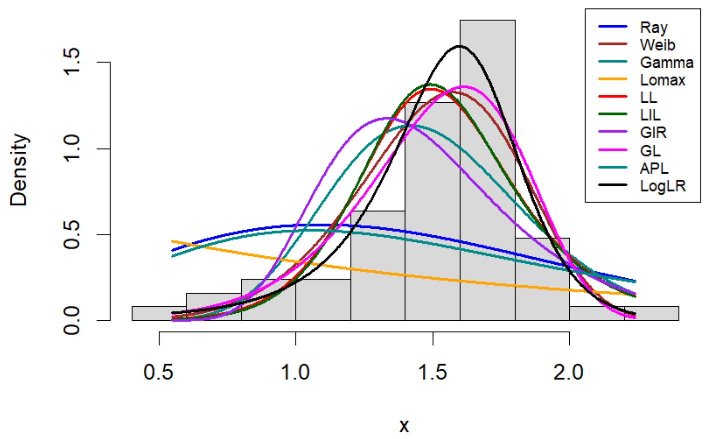

Figure 6. Fitted PDF curves for all competing models superimposed on the histogram for Dataset 1.

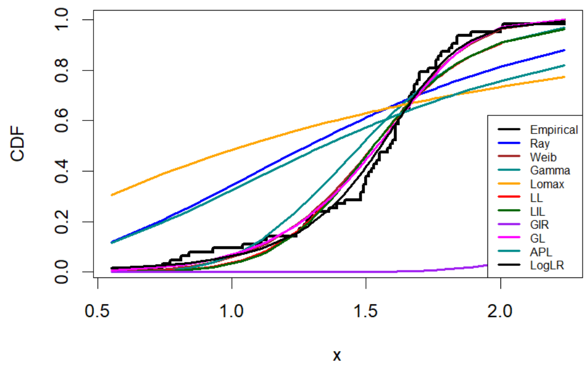

Figure 7. Empirical CDF of Dataset 1 and the fitted CDFs.

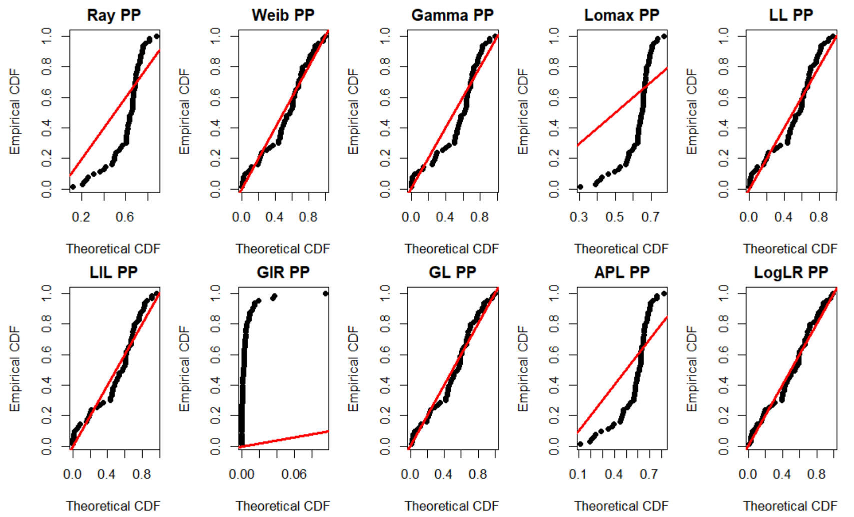

Figure 8. PP plot of all competing models for Dataset 1.

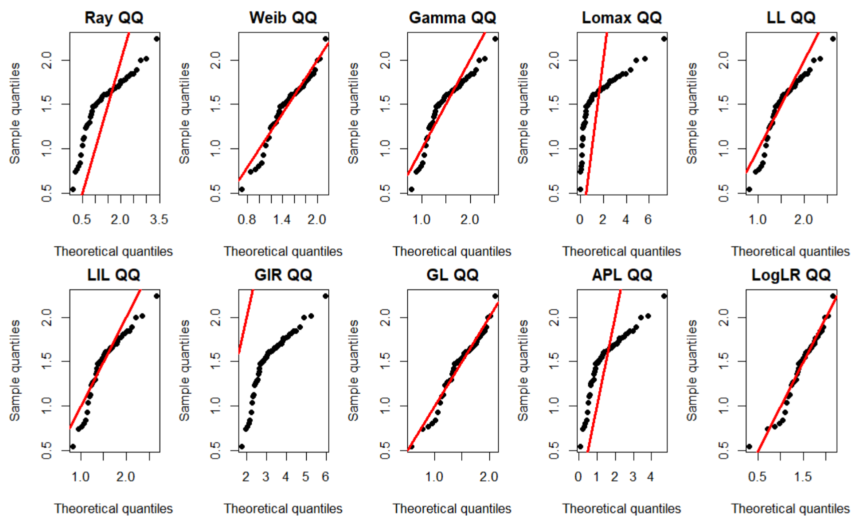

Figure 9. QQ plot of all competing models for Dataset 1.

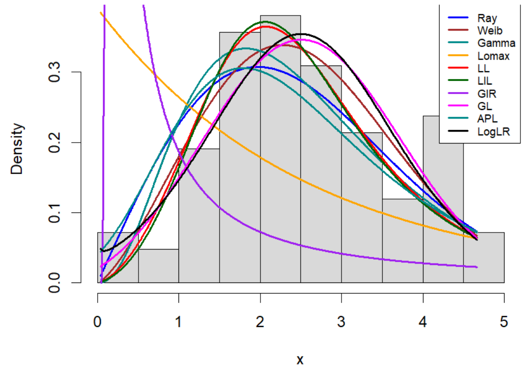

Figure 10. Fitted PDF curves for all competing models superimposed on the histogram of Dataset 2.

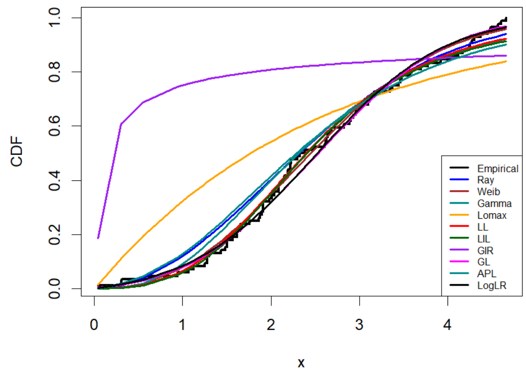

Figure 11. Empirical CDF of Dataset 2 and the fitted CDFs.

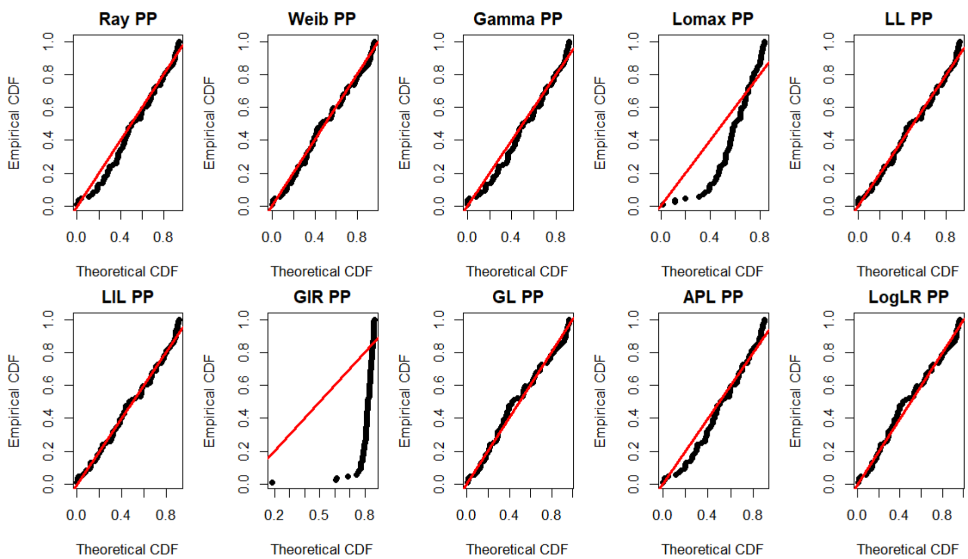

Figure 12. PP plot of all competing models for Dataset 2.

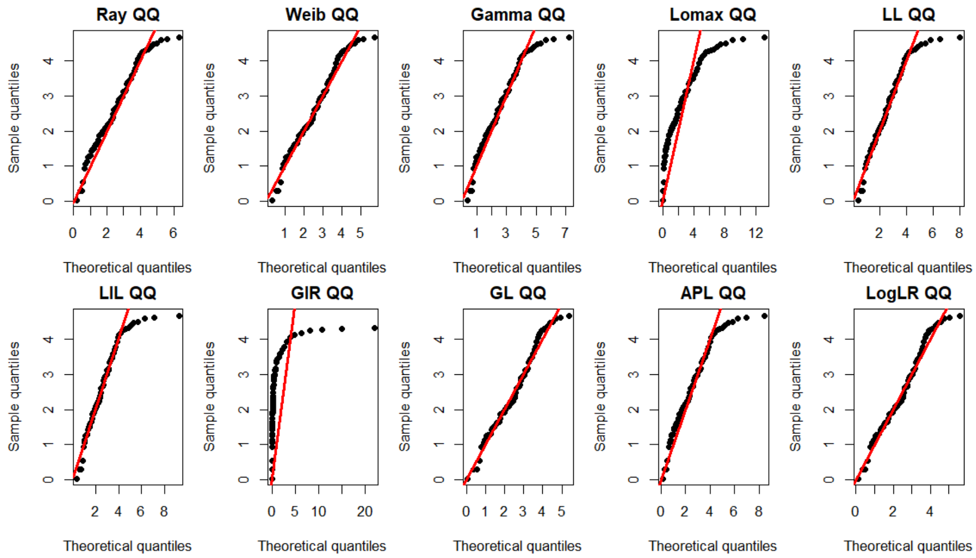

Figure 13. QQ plot of all competing models for Dataset 2.

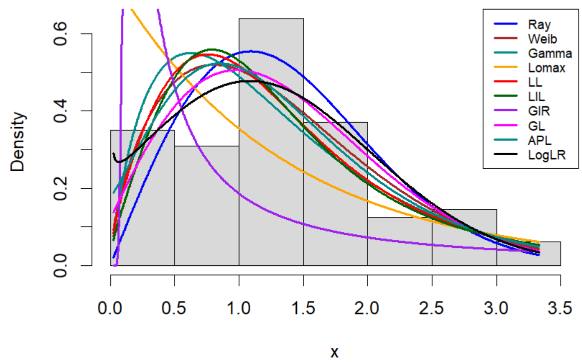

Figure 14. Fitted PDF curves for all competing models superimposed on the histogram of Dataset 3.

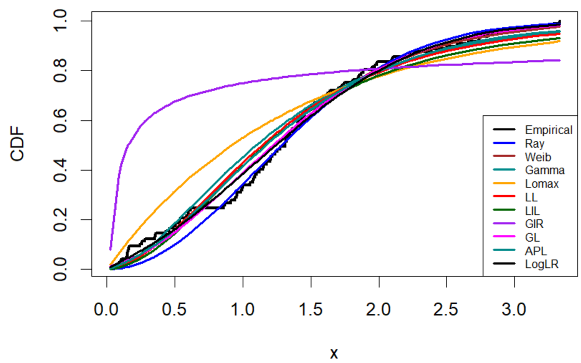

Figure 15. Empirical CDF of Dataset 3 and the fitted CDfs.

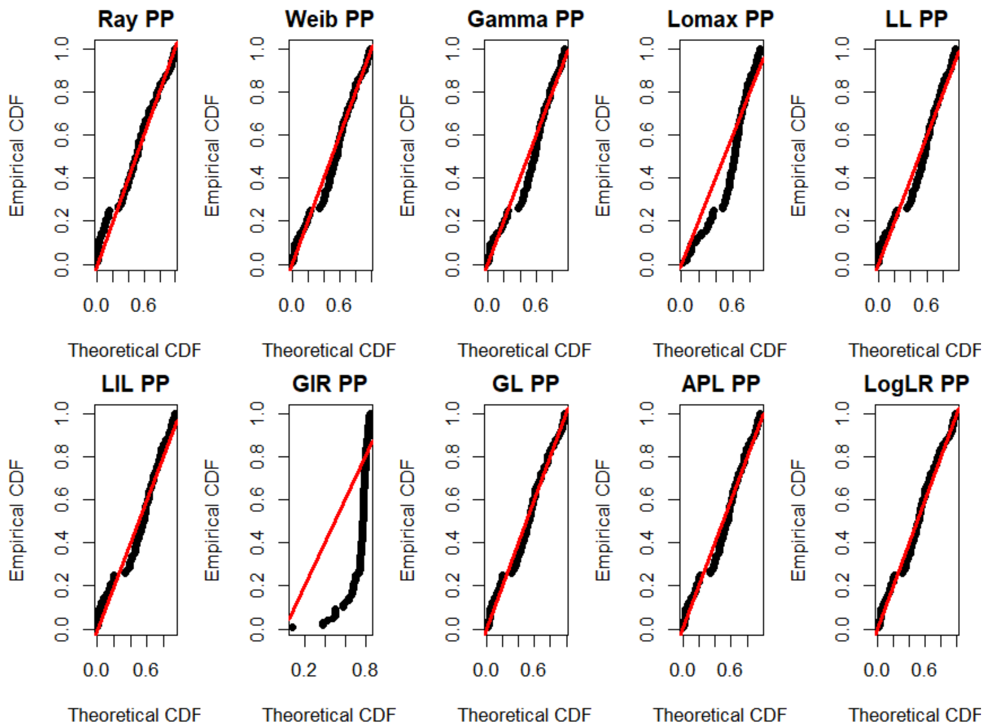

Figure 16. PP plot of all competing models for Dataset 3.

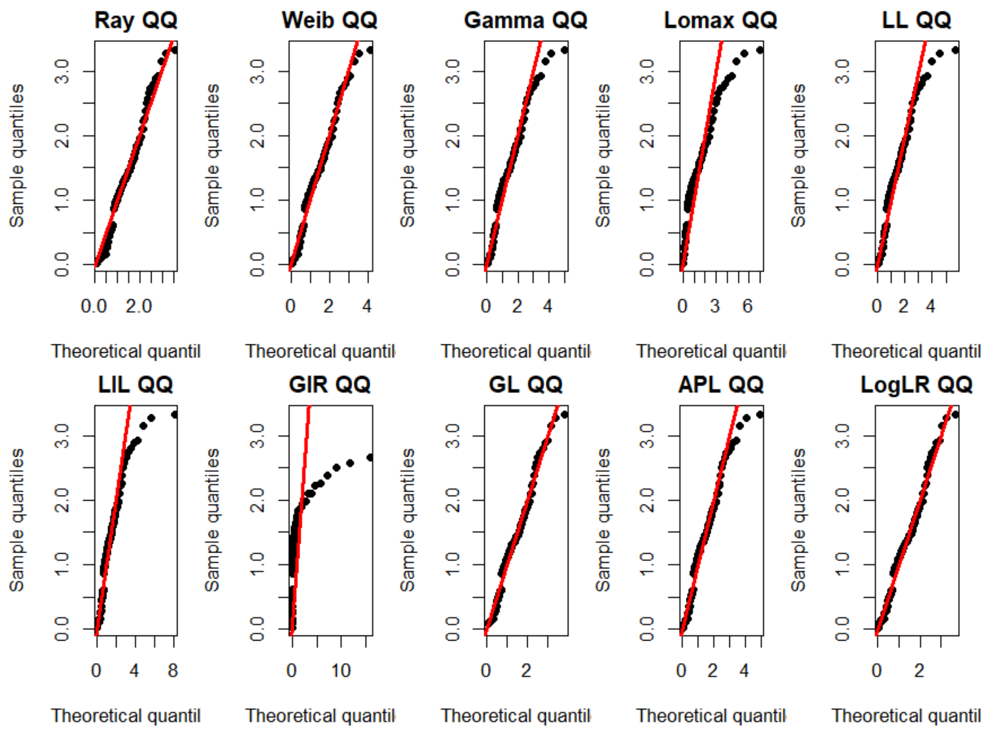

Figure 17. QQ plot of the Log-LR fit for Dataset 3.

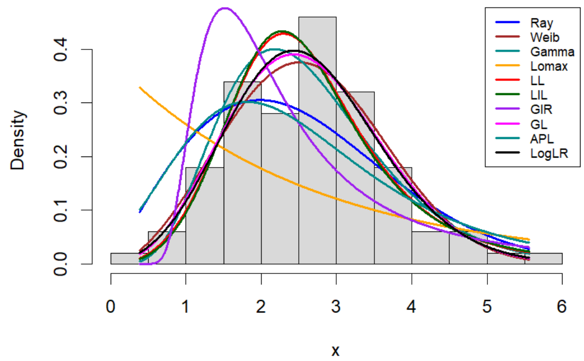

Figure 18. Fitted PDF curves for all competing models superimposed on the histogram of the Dataset 4.

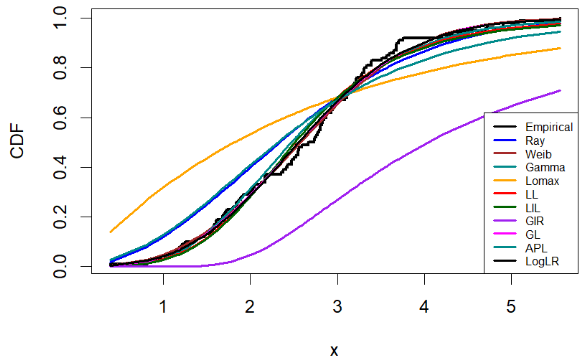

Figure 19. Empirical CDF of Dataset 4 and the fitted CDFs.

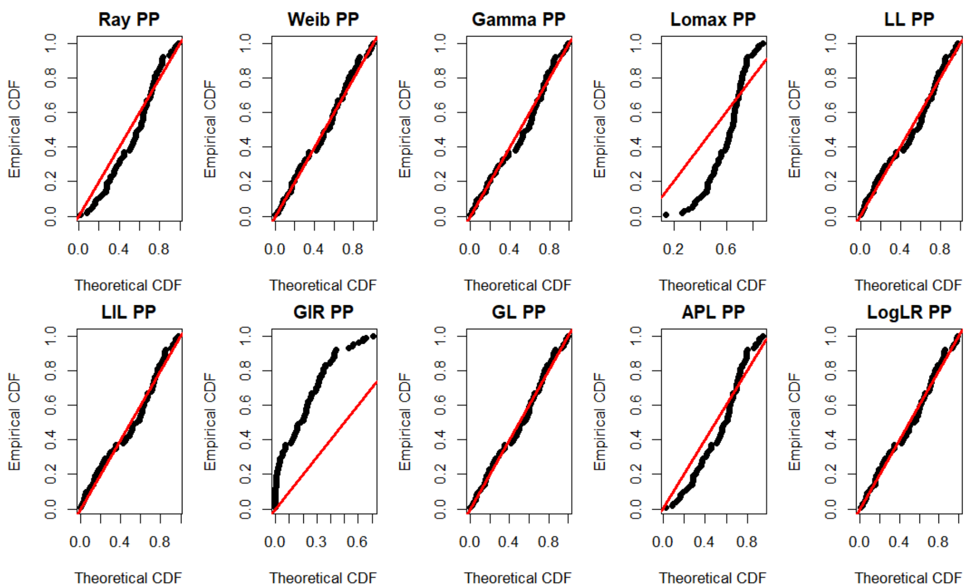

Figure 20. PP plot of all competing models for Dataset 4.

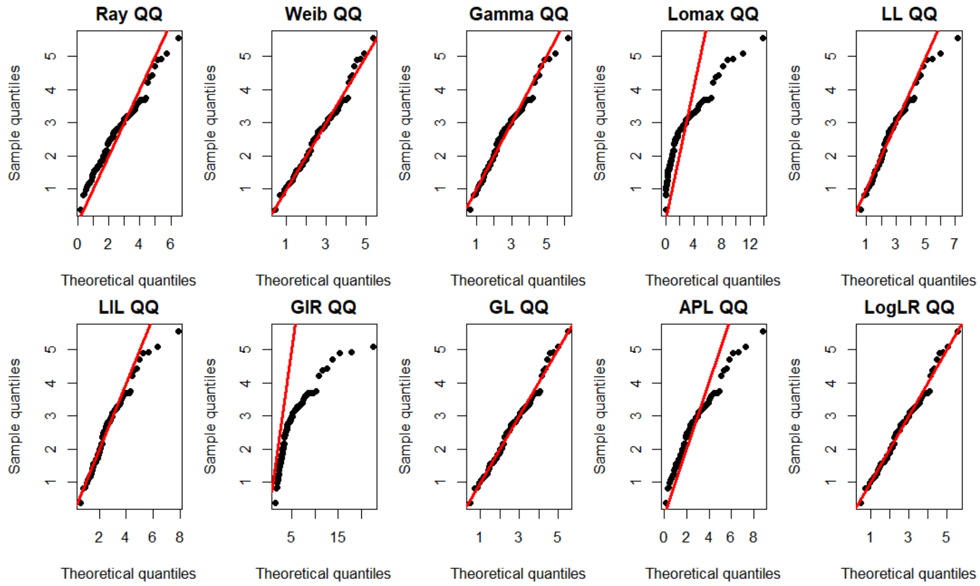

Figure 21. QQ plot of the Log-LR fit for Dataset 4.

Remark on numerical stability

It is noteworthy that some competing models yield extremely large parameter estimates. For example, the Lomax distribution fitted to Dataset 1 produces estimates of ($\hat{\alpha}$ = 27,804) and ($\hat{\lambda}$ = 41,907), while the APL model yields estimates that lie close to the boundary of the optimization region. Such behavior is unlikely to be due to computational issues; rather, it typically indicates weak parameter identifiability and a nearly flat likelihood surface in certain directions, where substantially different parameter combinations yield very similar likelihood values. This phenomenon is common in highly flexible or over-parameterized lifetime models when the available data do not contain sufficient information to stably estimate all parameters simultaneously. In contrast, the Log-LR model yields stable parameter estimates for Datasets 1–3, with SEs that remain moderately relative to the corresponding parameter values. For Dataset 4, the SEs of ($\hat{\alpha}$) and ($\hat{\beta}$) are larger, indicating greater uncertainty in estimating the shape components. This should be interpreted as reflecting limited local information in the likelihood rather than evidence of structural parameter dependence. Nevertheless, the scale parameter ($\hat{\lambda}$) is estimated with good precision across all four datasets, with ($\mathrm{SE}(\hat{\lambda})/\hat{\lambda} < 8\%$) in every case, supporting the numerical stability of the proposed model.

7. Conclusions

This study introduced the Log-LR distribution as a flexible three-parameter lifetime model within the Lomax-G family. Several of its statistical properties were derived, including closed-form expressions for the probability density, cumulative distribution, reliability, hazard rate, quantile, Shannon entropy, and MRL functions. In addition, the r-th moments and L-moments were expressed in integral form and evaluated numerically. The existence of the MGF was also established, implying the existence of all integer moments of the distribution.

The performance of the MLEs was investigated through an extensive Monte Carlo simulation study.

The results indicate that the estimators are consistent and exhibit satisfactory finite-sample behavior, with the bias, MSE, and MRE decreasing as the sample size increases. The practical usefulness of the proposed distribution was demonstrated using four real datasets from different application areas. Across all datasets, the Log-LR model consistently ranked among the best-performing models and frequently achieved the smallest values of the log-likelihood-based information criteria and goodness-of-fit statistics. In particular, it provided the best overall fit for most datasets while remaining highly competitive in the remaining cases. The graphical assessments based on fitted densities, empirical distribution functions, PP plots, and QQ plots further supported the adequacy of the proposed model.

Despite its favourable performance, several limitations should be acknowledged. First, the coverage probabilities of the Wald-type confidence intervals for $\hat{\lambda}$ remained below the nominal level under some parameter configurations, suggesting that profile-likelihood or bootstrap-based confidence intervals may provide more reliable inference. Second, for certain parameter combinations, the shape parameters α and β exhibited substantial interaction, which may result in relatively large SEs and reduced parameter identifiability.

Overall, the results demonstrate that the Log-LR distribution provides a flexible and useful framework for modeling lifetime data with decreasing hazard-rate behavior. Several directions for future research merit further investigation. These include the development of Bayesian estimation procedures, the construction of a Log-LR regression model that incorporates covariate information, and the extension of the proposed distribution to multivariate settings to model complex dependence structures in reliability, survival, and risk analysis applications. Furthermore, constructing confidence intervals for derived reliability quantities such as the reliability function $R(t)$, the hazard rate $h(t)$, and the mean time to failure using the delta method or parametric bootstrap is an important direction for future investigation.

Acknowledgments

The author would like to express sincere gratitude to the Editor and the reviewers for their valuable comments and constructive suggestions, which significantly improved the quality of this manuscript.

Use of Generative-AI tools declaration

The author declares that she has not used Artificial Intelligence (AI) tools in the creation of this article.

Conflict of interest

The author declares no conflict of interest.

References

1. N. Eugene, C. Lee, F. Famoye, Beta-normal distribution and its applications, *Commun. Stat. Theory Methods*, **31** (2002), 497–512. https://doi.org/10.1081/STA-120003130

2. A. W. Marshall, I. Olkin, A new method for adding a parameter to a family of distributions with application to the exponential and Weibull families, *Biometrika*, **92** (2005), 505. https://doi.org/10.1093/biomet/92.2.505
3. M. Alizadeh, F. Merovci, G. G. Hamedani, Generalized transmuted family of distributions: properties and applications, *Hacettepe J. Math. Stat.*, **46** (2017), 645–667.
4. M. Bourguignon, R. B. Silva, G. M. Cordeiro, The Weibull-G family of probability distributions, *J. Data Sci.*, **12** (2014), 53–68.
5. M. Alizadeh, G. M. Cordeiro, L. G. B. Pinho, I. Ghosh, The Gompertz-G family of distributions, *J. Stat. Theory Pract.*, **11** (2017), 179–207. https://doi.org/10.1080/15598608.2016.1267668
6. A. A. Al-Shomrani, A. J. Al-Arfaj, A new flexible odd Kappa-G family of distributions: theory and properties, *Adv. Appl. Math. Sci.*, **21** (2021), 3443–3514.
7. L. Anzagra, S. Sarpong, S. Nasiru, Odd Chen-G family of distributions, *Ann. Data Sci.*, **9** (2022), 369–391. https://doi.org/10.1007/s40745-020-00248-2
8. S. Benchiha, L. P. Sapkota, A. Al Mutairi, V. Kumar, R. H. Khashab, A. M. Gemeay, et al., A new sine family of generalized distributions: statistical inference with applications, *Math. Comput. Appl.*, **28** (2023), 83. https://doi.org/10.3390/mca28040083
9. M. Gabanakgosi, B. Oluyede, The Topp-Leone type II exponentiated half logistic-G family of distributions with applications, *Int. J. Math. Oper. Res.*, **25** (2023), 85–117. https://doi.org/10.1504/IJMOR.2023.131382
10. G. M. Cordeiro, E. M. M. Ortega, B. V. Popović, The gamma-Lomax distribution, *J. Stat. Comput. Simul.*, **85** (2015), 305–319. https://doi.org/10.1080/00949655.2013.822869
11. A. Alabid, A. A. Hurairah, The beta transmuted power distribution: properties and application, *Indones. J. Stat. Appl.*, **3** (2019), 105–123.
12. L. P. Sapkota, V. Kumar, A. M. Gemeay, M. E. Bakr, O. S. Balogun, A. H. Muse, New Lomax-G family of distributions: statistical properties and applications, *AIP Adv.*, **13** (2023), 095118. https://doi.org/10.1063/5.0171949
13. S. M. Zaidi, Z. Mahmood, M. N. Atchadé, Y. A. Tashkandy, M. E. Bakr, E. M. Almetwally, et al., Lomax tangent generalized family of distributions: characteristics, simulations, and applications on hydrological-strength data, *Heliyon*, **10** (2024), e32011. https://doi.org/10.1016/j.heliyon.2024.e32011
14. A. Fayomi, E. M. Almetwally, M. E. Qura, A novel bivariate Lomax-G family of distributions: properties, inference, and applications to environmental, medical, and computer science data, *AIMS Math.*, **8** (2023), 17539–17584. https://doi.org/10.3934/math.2023896
15. M. A. Abd Elgawad, M. A. Alawady, H. M. Barakat, G. M. Mansour, I. A. Husseiny, S. A. Alyami, et al., Bivariate power Lomax Sarmanov distribution: statistical properties, Reliability measures, and Parameter estimation, *Alex. Eng. J.*, **113** (2025), 593–610. https://doi.org/10.1016/j.aej.2024.10.074
16. A. Xu, Y. Miao, J. Sun, S. Zhou, Y. Tang, A hierarchical Bayesian multivariate Wiener process model with dependent degradation rates and volatilities, *IEEE Trans. Reliab.*, **75** (2026), 1420–1433. https://doi.org/10.1109/tr.2026.3674703

17. D. Zhu, A. Xu, Z. Chen, S. Ding, G. Fang, An online Bayesian framework for identifying latent system degradation states, *IEEE Trans. Reliab.*, **75** (2026), 542–554. https://doi.org/10.1109/tr.2025.3647489
18. A. Xu, Z. Chen, H. Yin, Y. Tang, A bivariate Wiener degradation model with partially random scale weights, *Reliab. Eng. Syst. Safety*, **275** (2026), 112684. https://doi.org/10.1016/j.ress.2026.112684
19. M. H. Tahir, M. A. Hussain, G. M. Cordeiro, G. G. Hamedani, M. Mansoor, M. Zubair, The Gumbel–Lomax distribution: properties and applications, *J. Stat. Theory Appl.*, **15** (2016), 61–79. https://doi.org/10.2991/jsta.2016.15.1.6
20. R. A. Bakoban, E. A. Faraj, N. S. Alsulami, A study on alpha power Lomax distribution, *Int. J. Eng. Sci. Technol.*, **6** (2022), 76–91. https://doi.org/10.29121/ijoest.v6.i5.2022.393
21. H. Baaqeel, H. Alnashri, A. S. Alghamdi, L. Baharith, A new Weibull–Rayleigh distribution: characterization, estimation methods, and applications with change point analysis, *Axioms*, **14** (2025), 649. https://doi.org/10.3390/axioms14090649
22. A. S. Malik, S. P. Ahmad, Generalized inverted Kumaraswamy–Rayleigh distribution: properties and application, *J. Mod. Appl. Stat. Methods*, **23** (2023). https://doi.org/10.56801/jmasm.v23.i1.15
23. J. R. M. Hosking, L-moments: analysis and estimation of distributions using linear combinations of order statistics, *J. R. Stat. Soc.: Ser. B (Methodol.)*, **52** (1990), 105–124. https://doi.org/10.1111/j.2517-6161.1990.tb01775.x
24. H. A. David, H. N. Nagaraja, *Order statistics*, 3 Eds., Wiley, 2003.
25. A. K. Chaudhary, V. Vijay Kumar, The logistic Lomax distribution with properties and applications, *Int. J. Stat. Appl. Math.*, **5** (2020), 12–19. https://doi.org/10.22271/maths.2020.v5.i6a.603
26. R. K. Joshi, V. Vijay Kumar, The logistic inverse Lomax distribution with properties and applications, *Int. J. Math. Comput. Res.*, **9** (2021), 2169–2177.
27. R. A. Bakoban, A. M. Al-Shehri, A new generalization of the generalized inverse Rayleigh distribution with applications, *Symmetry*, **13** (2021), 711. https://doi.org/10.3390/sym13040711
28. H. Baaqeel, H. Alnashri, L. Baharith, A new Lomax-G family: properties, estimation and applications, *Entropy*, **27** (2025), 125. https://doi.org/10.3390/e27020125
29. J. F. Lawless, *Statistical models and methods for lifetime data*, 2 Eds., Wiley, New York, 2011.
30. A. Alzaatreh, F. Famoye, C. Lee, The gamma-normal distribution: properties and applications, *Comput. Stat. Data Anal.*, **69** (2014), 67–80. https://doi.org/10.1016/j.csda.2013.07.035
31. M. Ijaz, M. Asim, A. Khalil, Flexible Lomax distribution, *Songklanakarin J. Sci. Technol.*, **42** (2020), 1125–1134.

Appendix

A. Derivation of the raw moments

In this Appendix, we provide the detailed derivation of the transformation used to obtain the alternative representation of the raw moments of the Log-LR distribution.

Starting from the r-th raw moment,

$$E(X^r) = \alpha\beta^\alpha \int_0^\infty \frac{x^{r+1} e^{-x^2/(2\lambda^2)}}{\lambda^2 \left(1 - e^{-x^2/(2\lambda^2)}\right)} [\eta(x)]^{-(\alpha+1)} dx,$$

we apply the transformation

$$y = -\log\left(1 - e^{-x^2/(2\lambda^2)}\right).$$

This implies

$$1 - e^{-x^2/(2\lambda^2)} = e^{-y}, \qquad e^{-x^2/(2\lambda^2)} = 1 - e^{-y}.$$

Solving for x^2 yields

$$x^2 = -2\lambda^2 \log(1 - e^{-y}),$$

and hence

$$x^r = (2\lambda^2)^{r/2} [-\log(1 - e^{-y})]^{r/2}.$$

A.1. Jacobian of the transformation

Differentiating the transformation gives

$$\begin{aligned} \frac{dy}{dx} &= -\frac{1}{1 - e^{-x^2/(2\lambda^2)}} \cdot \frac{d}{dx}\left(1 - e^{-x^2/(2\lambda^2)}\right) \\ &= -\frac{x}{\lambda^2} \frac{e^{-x^2/(2\lambda^2)}}{1 - e^{-x^2/(2\lambda^2)}}, \end{aligned}$$

so that

$$dy = -\frac{x}{\lambda^2} \frac{e^{-x^2/(2\lambda^2)}}{1 - e^{-x^2/(2\lambda^2)}} \, dx.$$

A.2. Change of limits

The transformation of the integration limits is given by

$$x \to 0^+ \implies y \to \infty, \qquad x \to \infty \implies y \to 0.$$

Reversing the limits removes the negative sign in the Jacobian.

A.3. Final transformed form

Substituting the above results into the moment expression yields

$$E(X^r) = \alpha\beta^\alpha (2\lambda^2)^{r/2} \int_0^\infty [-\log(1 - e^{-y})]^{r/2} (\beta + y)^{-(\alpha+1)} \, dy.$$

A.4. Series representation

Using the known expansion

$$-\log(1-e^{-y}) = \sum_{k=1}^{\infty} \frac{e^{-ky}}{k}, \qquad y > 0,$$

we obtain

$$[-\log(1-e^{-y})]^{r/2} = \left(\sum_{k=1}^{\infty} \frac{e^{-ky}}{k}\right)^{r/2}.$$

For general r, this expression yields nested infinite series upon expansion and does not reduce to a finite closed-form expression in terms of standard functions. Therefore, numerical integration or truncated series approximations are required in practice.

B. Derivation of the score functions and observed information matrix

This Appendix provides the detailed derivations of the score functions and the elements of the observed information matrix used in the maximum-likelihood estimation procedure. For notational convenience, define

$$t_i = \frac{x_i^2}{2\lambda^2}, \qquad F_i = 1 - e^{-t_i}, \qquad \eta_i = \beta - \log(F_i),$$

and

$$w_i = \frac{e^{-t_i}}{F_i}.$$

The derivation proceeds by first obtaining the score functions and subsequently differentiating them to derive the elements of the observed information matrix.

B.1. Useful derivatives

The following identities are repeatedly used throughout the derivations:

$$\begin{aligned}
\frac{\partial t_i}{\partial \lambda} &= -\frac{x_i^2}{\lambda^3},\\
\frac{\partial F_i}{\partial \lambda} &= \frac{\partial}{\partial \lambda}(1 - e^{-t_i}) = e^{-t_i}\frac{\partial t_i}{\partial \lambda} = -\frac{x_i^2}{\lambda^3} e^{-t_i},\\
\frac{\partial \log(F_i)}{\partial \lambda} &= \frac{1}{F_i}\frac{\partial F_i}{\partial \lambda} = -\frac{x_i^2}{\lambda^3}\frac{e^{-t_i}}{F_i} = -\frac{x_i^2}{\lambda^3} w_i,\\
\frac{\partial \eta_i}{\partial \lambda} &= -\frac{\partial}{\partial \lambda}\log(F_i) = \frac{x_i^2}{\lambda^3} w_i.
\end{aligned}$$

B.2. Derivation of the score functions

The log-likelihood function is

$$\ell(\omega) = n\log\alpha + n\alpha\log\beta + \sum_{i=1}^{n}\log x_i - \frac{1}{2\lambda^2}\sum_{i=1}^{n}x_i^2$$
$$- n\log\lambda^2 - \sum_{i=1}^{n}\log(F_i) - (\alpha+1)\sum_{i=1}^{n}\log(\eta_i).$$

B.2.1. Derivative with respect to α

Collecting all terms involving α,

$$\ell(\alpha) = n\log\alpha + n\alpha\log\beta - (\alpha+1)\sum_{i=1}^{n}\log(\eta_i).$$

Differentiating gives

$$\frac{\partial\ell}{\partial\alpha} = \frac{n}{\alpha} + n\log\beta - \sum_{i=1}^{n}\log(\eta_i).$$

Differentiating once more,

$$\frac{\partial^2\ell}{\partial\alpha^2} = -\frac{n}{\alpha^2}.$$

B.2.2. Derivative with respect to β

Since

$$\frac{\partial\eta_i}{\partial\beta} = 1,$$

we have

$$\frac{\partial}{\partial\beta}\log(\eta_i) = \frac{1}{\eta_i}.$$

Therefore,

$$\frac{\partial\ell}{\partial\beta} = \frac{n\alpha}{\beta} - (\alpha+1)\sum_{i=1}^{n}\frac{1}{\eta_i}.$$

Differentiating again,

$$\frac{\partial^2\ell}{\partial\beta^2} = -\frac{n\alpha}{\beta^2} + (\alpha+1)\sum_{i=1}^{n}\frac{1}{\eta_i^2}.$$

B.2.3. Derivative with respect to λ

Differentiating each λ-dependent term separately,

$$\frac{\partial}{\partial\lambda}\left(-n\log\lambda^2\right) = -\frac{2n}{\lambda},$$

and

$$\frac{\partial}{\partial\lambda}\left(-\frac{1}{2\lambda^2}\sum_{i=1}^{n}x_i^2\right)=\frac{1}{\lambda^3}\sum_{i=1}^{n}x_i^2.$$

Next,

$$\frac{\partial}{\partial\lambda}\left[-\sum_{i=1}^{n}\log(F_i)\right]=\frac{1}{\lambda^3}\sum_{i=1}^{n}x_i^2w_i.$$

Furthermore,

$$\frac{\partial}{\partial\lambda}\left[-(\alpha+1)\sum_{i=1}^{n}\log(\eta_i)\right]=-\frac{\alpha+1}{\lambda^3}\sum_{i=1}^{n}\frac{x_i^2w_i}{\eta_i}.$$

Combining all contributions yields

$$\begin{aligned}\frac{\partial\ell}{\partial\lambda}=-\frac{2n}{\lambda}+\frac{1}{\lambda^3}\sum_{i=1}^{n}x_i^2+\frac{1}{\lambda^3}\sum_{i=1}^{n}x_i^2w_i\\ -\frac{\alpha+1}{\lambda^3}\sum_{i=1}^{n}\frac{x_i^2w_i}{\eta_i}.\end{aligned}$$

B.3. Mixed derivatives

Differentiating the score functions with respect to the remaining parameters gives

$$\frac{\partial^2\ell}{\partial\alpha\,\partial\beta}=\frac{n}{\beta}-\sum_{i=1}^{n}\frac{1}{\eta_i},$$

$$\frac{\partial^2\ell}{\partial\alpha\,\partial\lambda}=-\frac{1}{\lambda^3}\sum_{i=1}^{n}\frac{x_i^2w_i}{\eta_i},$$

$$\frac{\partial^2\ell}{\partial\beta\,\partial\lambda}=\frac{\alpha+1}{\lambda^3}\sum_{i=1}^{n}\frac{x_i^2w_i}{\eta_i^2}.$$

B.4. Second derivative with respect to λ

Differentiating the score function $\partial\ell/\partial\lambda$ term by term yields

$$\begin{aligned}\frac{\partial^2\ell}{\partial\lambda^2}=\frac{2n}{\lambda^2}-\frac{3}{\lambda^4}\sum_{i=1}^{n}x_i^2-\frac{3}{\lambda^4}\sum_{i=1}^{n}x_i^2w_i+\frac{1}{\lambda^6}\sum_{i=1}^{n}\frac{x_i^4e^{-t_i}}{F_i^2}\\ +\frac{3(\alpha+1)}{\lambda^4}\sum_{i=1}^{n}\frac{x_i^2w_i}{\eta_i}-\frac{\alpha+1}{\lambda^6}\sum_{i=1}^{n}\frac{x_i^4e^{-t_i}}{F_i^2\eta_i}\\ +\frac{\alpha+1}{\lambda^6}\sum_{i=1}^{n}\frac{x_i^4w_i^2}{\eta_i^2}.\end{aligned}$$

Consequently, the observed information matrix is obtained by evaluating the negative Hessian matrix at the MLEs

$$\mathbf{I}(\widehat{\omega}) = -\left[\frac{\partial^2 \ell}{\partial\omega_i \partial\omega_j}\right]_{\omega=\widehat{\omega}}.$$

The inverse of the observed information matrix yields the asymptotic variance-covariance matrix of the MLEs.